Cell

A circadian rheostat drives proton electrochemical gradients to optimize cell-type-specific growth in *Arabidopsis*

Graphical abstract

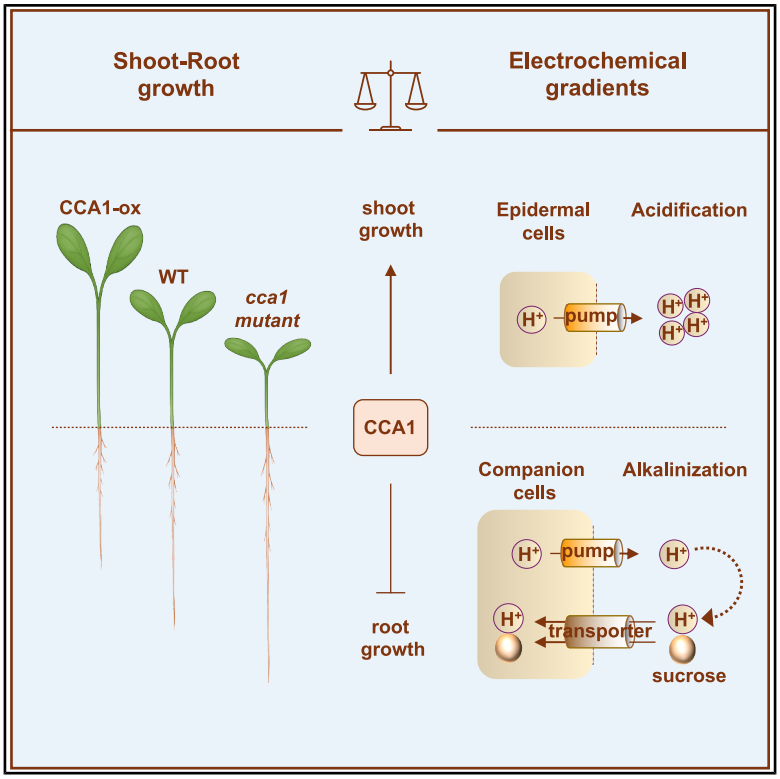

Highlights

- Antiphasic oscillation of apoplastic pH in epidermal and phloem companion cells
- CCA1 lowers apoplastic pH in epidermal cells and promotes hypocotyl growth
- CCA1 represses the H^+-pump *AHA3*, raising phloem apoplastic pH and reducing root growth
- CCA1-mediated phloem pH changes affect sucrose loading, balancing shoot-root growth

Authors

Lu Xiong, Motohide Seki, Akiko Satake, Paloma Mas

Correspondence

paloma.mas@cragenomica.es

In brief

The clock component CCA1 functions as a molecular rheostat, fine-tuning cell-type-specific electrochemical gradients to optimize carbon allocation and the timely coordination of shoot and root growth balance.

Xiong et al., 2026, Cell *189*, 1–17
March 19, 2026
https://doi.org/10.1016/j.cell.2025.12.056

CellPress

Please cite this article in press as: Xiong et al., A circadian rheostat drives proton electrochemical gradients to optimize cell-type-specific growth in *Arabidopsis*, Cell (2026), https://doi.org/10.1016/j.cell.2025.12.056

Cell

CellPress
OPEN ACCESS

Article

A circadian rheostat drives proton electrochemical gradients to optimize cell-type-specific growth in *Arabidopsis*

Lu Xiong,[1] Motohide Seki,[2] Akiko Satake,[3] and Paloma Mas[1,4,5,6,*]

[1]Centre for Research in Agricultural Genomics (CRAG), CSIC, IRTA-UAB-UB, Campus UAB, 08193 Barcelona, Spain
[2]Faculty of Design, Kyushu University, 4-9-1 Shiobaru, Minamiku, Fukuoka 815-8540, Japan
[3]Department of Biology, Faculty of Science, Kyushu University, 744 Motooka, Nishi-ku, Fukuoka 819-0395, Japan
[4]Consejo Superior de Investigaciones Científicas (CSIC), 08028 Barcelona, Spain
[5]Senior author
[6]Lead contact
*Correspondence: paloma.mas@cragenomica.es
https://doi.org/10.1016/j.cell.2025.12.056

SUMMARY

Plant growth relies on the activity of key transcription factors. Here, we uncover a mechanism for organ-specific growth driven by opposing electrochemical signals that propagate in a cell-type-specific manner. Using a genetically encoded pH sensor and a pH-sensitive dye, we show that apoplastic pH in epidermal cells oscillates antiphasically relative to phloem pH. The clock component CCA1 lowers apoplastic pH in hypocotyl epidermal cells while increasing it in companion cells. This opposing regulation promotes hypocotyl growth but inhibits root elongation. Mechanistically, CCA1 activates auxin signaling in shoots while repressing *sucrose transporter 2* and the electrogenic (H^+)-pump ATPase *AHA3* by directly binding their promoters. The repression decreases sucrose loading into the phloem and slows transport velocity. Expressing CCA1 in the phloem is sufficient to inhibit root elongation, whereas AHA3 overexpression in CCA1 overexpressing seedlings rescues root growth. Thus, a circadian rheostat orchestrates electrochemical signals to optimize source capacity with sink demand.

INTRODUCTION

The circadian clock is one of the main components governing growth.[1–4] Rhythmic elongation of hypocotyls, the embryonic stems, depends on the timely control of growth master regulators such as PHYTOCHROME INTERACTING FACTOR 4 (PIF4) and PIF5.[5,6] Consequently, mis-expression of clock components can lead to severe growth phenotypes.[1–4] For example, CIRCADIAN CLOCK ASSOCIATED 1 over-expressing (CCA1-ox) seedlings display a long hypocotyl phenotype,[7] which suggests a growth-promoting role for CCA1. Regulation of hypocotyl growth by CCA1 relies on multiple entry points as CCA1 activates PIFs and interacts with auxin-related proteins.[8–10] The circadian clock is also connected with root growth, although the molecular mechanisms are not fully understood. Early studies showed that proper circadian function and *CCA1* expression are necessary for root length and architecture.[11] The circadian clock also plays an important role in controlling lateral root emergence by gating auxin signaling.[12] Light in shoots is able to generate rhythms in root hairs,[13] while root-to-shoot signaling enhances the accuracy of the shoot circadian clock.[14]

The acid growth theory proposes that auxin-induced apoplast acidification promotes cell wall loosening, thereby facilitating cell elongation.[15–21] The plasma membrane (H^+)-ATPases are key drivers of this apoplast acidification, coupling ATP hydrolysis with proton pumping from the cytoplasm into the extracellular space.[22] This scalar and vectorial activity generates proton electrochemical gradients across the plasma membrane, providing the motive force that drives carriers and channels.[23] Plants and fungi have some of the highest membrane potentials found in nature.[24] In *Arabidopsis thaliana*, the P-type plasma membrane H^+-ATPases (*Arabidopsis* H^+ ATPases, AHAs) comprise a multi-gene family with distinct expression patterns, kinetics, and specialized functions.[23,25] The closely related genes *AHA1* and *AHA2* are the most highly expressed isoforms[24] and have been extensively characterized. Molecular genetic approaches have proven their implication in a wide range of processes, including nutrient uptake, pollen development, stomatal opening, carbon-water usage, leaf hydraulics, or stress responses.[26–31] On the other hand, a null *AHA3* mutant is male-gametophytic lethal.[32] AHA3 is localized in the companion cells of the phloem and in reproductive tissues,[33,34] and it plays a role in pollen development,[32,35] in growth,[36] and in leaf vein mechano-sensing.[27] AHA3 is co-expressed with genes involved in sucrose phloem loading, such as *SUCROSE2* (*SUC2*).[23] Consistently, co-suppression of (H^+)-ATPase impairs sucrose loading and translocation to the sink tissues by altering

Please cite this article in press as: Xiong et al., A circadian rheostat drives proton electrochemical gradients to optimize cell-type-specific growth in *Arabidopsis*, Cell (2026), https://doi.org/10.1016/j.cell.2025.12.056

the electric potential and pH gradient required for phloem loading and solute transport.[23,37]

The primary photoassimilate in vascular plants, sucrose, is transported from source to sink tissues,[38] providing biomass for growth and storage and acting as a signaling molecule for growth.[39] Sucrose transport is a dynamic process influenced by developmental stage, metabolic status, light, and hormonal signals.[38] The uptake of sucrose from the apoplast of source tissues into companion cells and sieve elements is mediated by sucrose transporters (SUTs/SUCs).[40] These transporters function as sucrose/proton symporters that utilize the proton motive force generated by plasma membrane H^+-ATPases to load sucrose against a concentration gradient. SUC2 encodes the predominant carrier catalyzing phloem loading in *Arabidopsis*.[41] Phloem-loaded sucrose acts as a long-distance signal that controls growth in sink tissues such as roots.[42] Consequently, loss-of-function mutants of *SUTs/SUCs* with reduced phloem loading and altered sucrose distribution show growth defects.[41] Proper carbon partitioning is thus essential for balancing growth between source and sink organs. Misregulation of carbon distribution can result in growth imbalances, which underscores the importance of maintaining source-to-sink homeostasis for overall plant growth and productivity.[43] The regulatory network underlying this balance is complex and ultimately aids in the modulation of both source activity and sink strength.[38]

RESULTS

Organ-specific role of CCA1 in the control of growth

CCA1-ox seedlings grown under constant light (LL) conditions without prior entrainment showed significantly longer hypocotyls than wild type (WT), while a *cca1lhy* double mutant displayed the opposite phenotype (Figures 1A and S1A). Under our growing conditions, the CCA1-ox hypocotyls were even longer than those of the *elf3* mutant (Figure 1A) and the clock-related *prr* (*pseudo-response regulator)* higher-order mutants (Figure 1B). Altered growth was observed at several light intensities but was slightly more pronounced under low light (5 and 15 μE) (Figures 1C–1E and S1B–S1D). CCA1-ox and *cca1lhy* seedlings also displayed growth phenotypes under light-dark (LD) cycles (Figures 1F and S1E). However, compared to the WT, no significant differences were observed under constant darkness (DD) (Figure S1F). The results assign a role for CCA1 in promoting hypocotyl growth and indicate that CCA1-ox might be hyposensitive and *cca1lhy* hypersensitive to the light-mediated inhibition of hypocotyl growth.

Further analyses revealed opposite phenotypes in roots compared with those observed in hypocotyls. CCA1-ox plants exhibited short primary roots, while the *cca1lhy* mutant displayed long roots compared with WT (Figure 1G). These root growth phenotypes were consistent across various light intensities (Figures 1G, S1G, and S1H) but were not observed under DD (Figure 1H). CCA1-ox roots remained shorter and *cca1lhy* roots longer when roots were kept in darkness while the hypocotyls were exposed to light (dark roots, DR) (Figure S1I). Time-course analyses over a diel cycle of plants grown under low light intensity (15 μE) showed an oscillatory waveform of root growth in WT plants that dampened low in CCA1-ox (Figure S1J). The results confirmed that circadian timing mediated by CCA1 is important to control root growth. Developmental time-course analyses of hypocotyl and root growth also revealed that the growth phenotypes appeared at early stages of development (Figures 1I, 1J, and S1K–S1M). The opposed growth phenotypes consequently led to hypocotyl-to-root length ratios that were significantly increased in CCA1-ox plants and decreased in *cca1lhy* mutants compared with the WT (Figure 1K). The organ-specific inverse regulation of growth does not appear to be a general mechanism of balancing growth. For example, mutants with inherently long hypocotyls, such as *elf3*, did not exhibit correspondingly shorter roots. Unlike CCA1-ox and *cca1lhy*, the *elf3* mutant displayed parallel growth phenotypes in both hypocotyls and roots, albeit more prominently in hypocotyls (Figure 1K). Graphing the growth ratio relative to the WT highlights the organ-specific inverse phenotypes of CCA1 misexpressing plants (Figure 1L).

Organ-specific transcriptional network regulated by CCA1

RNA sequencing (RNA-seq) analyses of shoots and roots uncovered the transcriptional network underlying the organ-specific function of CCA1. Analyses of differentially expressed genes (DEGs) in CCA1-ox compared with WT revealed a higher number of upregulated genes in shoots in contrast to the increased number of downregulated genes in roots (Figures 2A, 2B, S2A, and S2B; Table S1). The expression of DEGs showed good reproducibility across the replicates for each genotype (Figures 2C and 2D). Using available circadian datasets (diurnal), we identified rhythmic oscillation in approximately 95% of the DEGs in both shoots and roots (Table S1). Compared with the expected counts (enriched at midday and midnight), peak phases of DEGs in shoots were additionally enriched at dawn and dusk (Figure 2E) and at midday and dusk for roots (Figure 2F). The results suggest that CCA1's role within the circadian clock might drive most of the transcriptional changes.

Comparing DEGs in shoots and roots revealed common as well as organ-specific DEGs (Figure 2G). Gene Ontology (GO)-term analyses of shoot-specific DEGs (DEGs SHs) showed a significant enrichment in auxin-related genes that were specifically upregulated in CCA1-ox shoots. The results agreed with studies showing that CCA1 gates the auxin signaling pathway.[8–10] Some of the auxin-related genes, such as *SAUR22* (*SMALL AUXIN-UP RNA 22*), were not expressed in roots (Figure S2C), or when expressed, such as *YUC8* (*YUCCA8*), they were not differential in WT and CCA1-ox roots (Figure 2H). Shoot-specific DEGs included known targets such as *PIF4* and *PIF5* that were significantly upregulated in CCA1-ox shoots but minimally expressed in roots, as previously described[45] (Figures 2I and S2D).

Organ-specific chromatin immunoprecipitation (ChIP) assays demonstrated CCA1 binding to the *PIF4* gene promoter in shoots but not in roots (Figure 2J). ChIP assays performed with plants expressing *CCA1* under its promoter (CCA1 Minigene, CMG) showed similar organ-specific binding (Figure 2K). ChIP enrichment of the *TOC1* (*TIMING OF CAB EXPRESSION 1*) promoter, a known target of CCA1, was observed in both shoots and roots (Figures 2J and 2K), which validated the reliability of our ChIP assays. Only background enrichment was found

Please cite this article in press as: Xiong et al., A circadian rheostat drives proton electrochemical gradients to optimize cell-type-specific growth in *Arabidopsis*, Cell (2026), https://doi.org/10.1016/j.cell.2025.12.056

CellPress
OPEN ACCESS

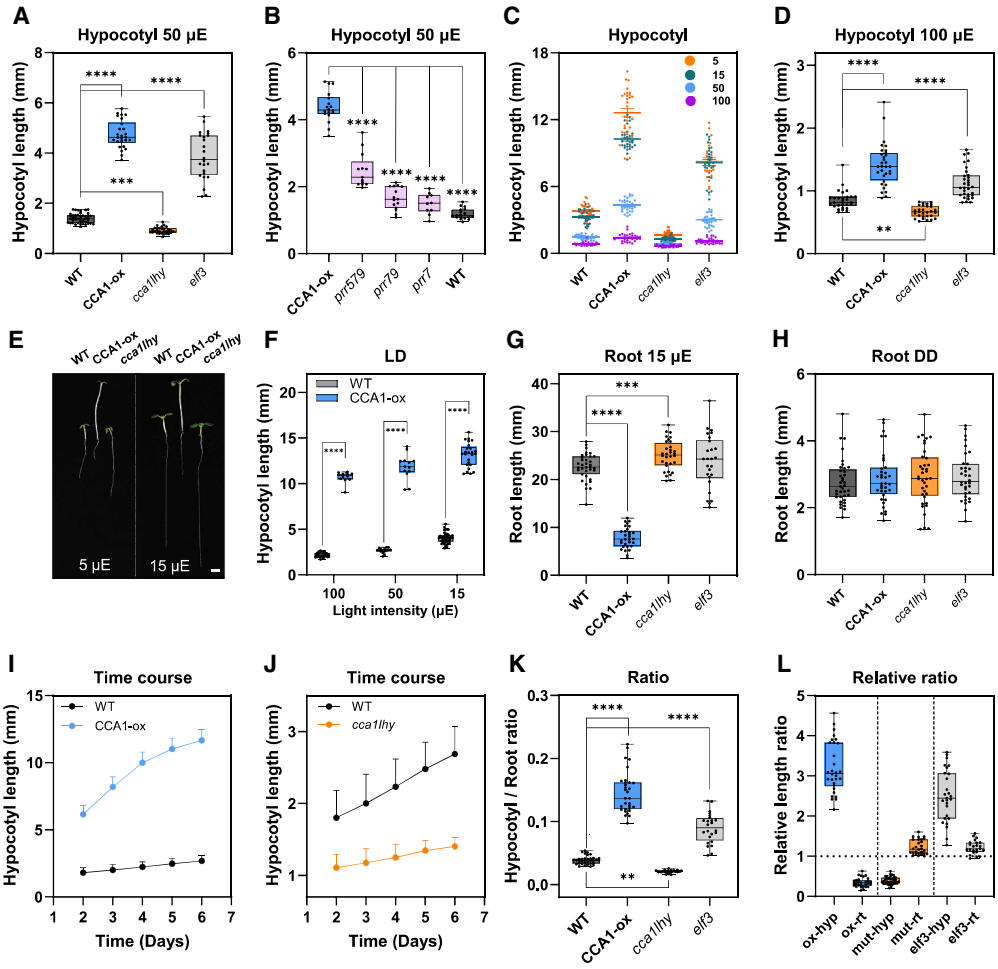

Figure 1. Organ-specific role of CCA1 in the control of growth

(A and B) Hypocotyl length of (A) WT, CCA1-ox, *cca1lhy*, and *elf3*, and (B) *prr579*, *prr79*, and *prr7* mutants grown under LL at 50 µE light intensity.

(C) Differential hypocotyl elongation responses of WT, CCA1-ox, *cca1lhy*, and *elf3* seedlings under varying light fluences (100, 50, 15, and 5 µE).

(D) Hypocotyl length of WT, CCA1-ox, *cca1lhy*, and *elf3* seedlings grown under LL at 100 µE light intensity.

(E) Representative image of WT, CCA1-ox, and *cca1lhy* seedlings grown under LL at 5 and 15 µE light intensity. Scale bar, 2 mm.

(F) Hypocotyl length of WT and CCA1-ox seedlings grown under LD at 100, 50, and 15 µE light intensity.

(G) Primary root length of WT, CCA1-ox, *cca1lhy*, and *elf3* seedlings grown under LL at 15 µE.

(H–J) (H) Primary root length of WT, CCA1-ox, *cca1lhy*, and *elf3* seedlings grown under DD. Time-course analyses of hypocotyl growth under LL at 15 µE light intensity of (I) WT and CCA1-ox and (J) WT and *cca1lhy* (day 1 represents the day of cotyledon emergence from the seed coat). Data are shown as the mean + SD of three independent experiments.

(K) Hypocotyl-to-root length ratio of WT, CCA1-ox, *cca1lhy*, and *elf3* seedlings grown under LL at 50 µE light intensity.

(L) Organ length ratio of each genotype relative to WT seedlings grown under LL at 15 µE light intensity.

The boxplots display the median and interquartile range, with the whiskers extending to the data range (minimum to maximum). **** p value $\leq$ 0.0001; *** p value $\leq$ 0.0002; ** p value $\leq$ 0.008. At least 12 seedlings were assayed per experiment with three biologically independent replicates.

See also Figure S1.

when amplifying the transcriptionally inactive retrotransposon *TA3* used as a negative control (Figures 2J and 2K). The results indicate that CCA1 binds to the *PIF4* promoter specifically in shoots, activating its expression in shoots but not in roots. Our results are in line with previous studies[9,10] showing that the direct activation of *PIF4* and the auxin signaling pathway by CCA1 might contribute to the promotion of hypocotyl growth. Our data further expand these findings by providing evidence for the organ-specific regulation of *PIF4* by CCA1.

Shoots and roots common DEGs (Figure 2G, common) were significantly enriched in the circadian signaling pathway, regulation of circadian processes, responses to light and abiotic stimulus, and development (Figure 2L). The common DEGs included many core oscillator genes in which CCA1 appeared as a repressor in both shoots and roots (Figures S2E–S2I). In WT plants, the overall expression of morning-core clock genes such as *LHY* (*LATE ELONGATED HYPOCOTYL*) or *RVE8* (*REVEILLE 8*) was reduced in roots compared with shoots, while

Please cite this article in press as: Xiong et al., A circadian rheostat drives proton electrochemical gradients to optimize cell-type-specific growth in *Arabidopsis*, Cell (2026), https://doi.org/10.1016/j.cell.2025.12.056

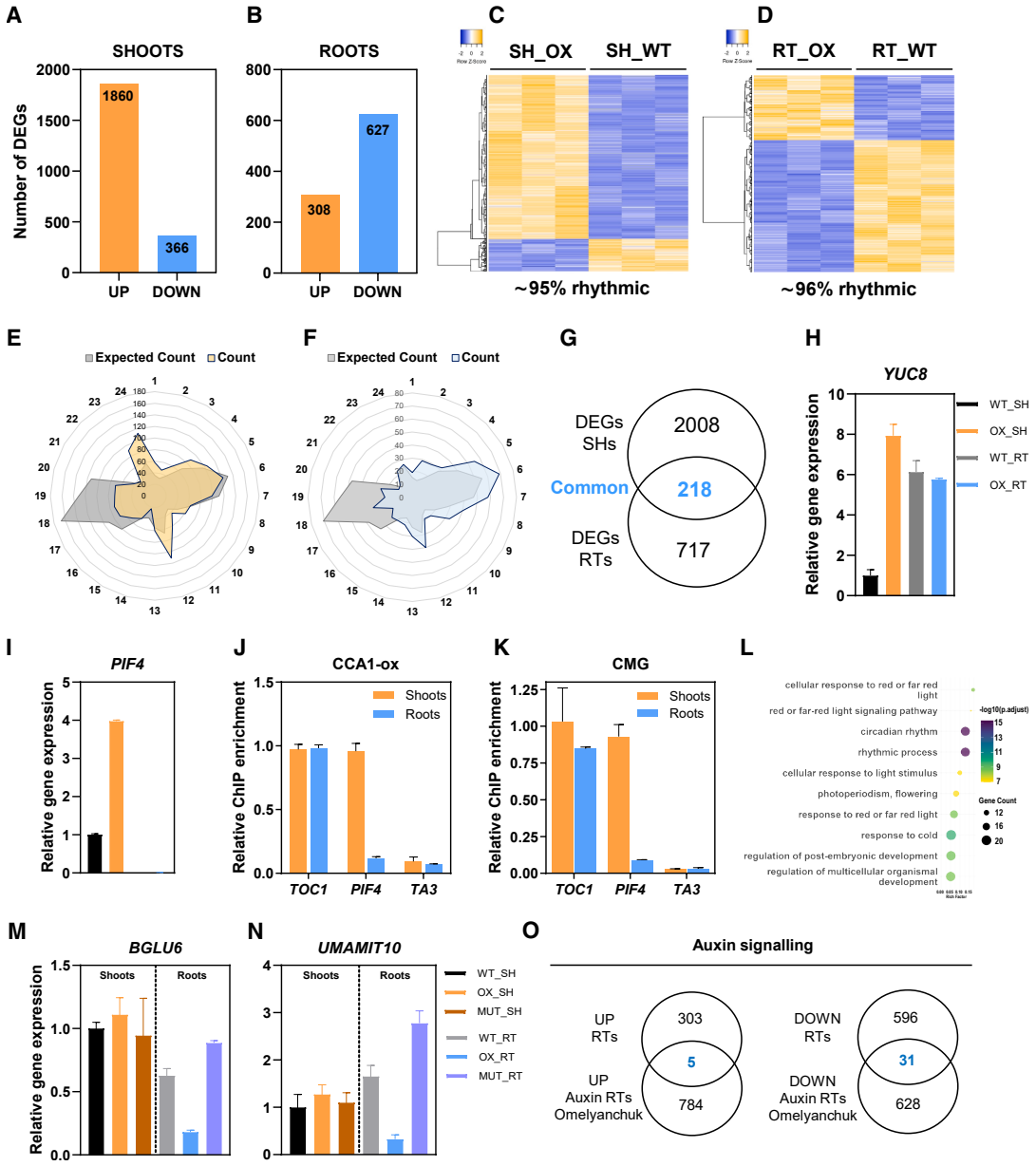

Figure 2. Organ-specific transcriptional network regulated by CCA1

(A–F) Up- and down-regulated DEGs in CCA1-ox relative to the WT from RNA-seq analyses of (A) shoots and (B) roots. Heatmap of DEG expression of WT and CCA1-ox (OX) in (C) shoots (SH_WT, SH_OX) and (D) roots (RT_WT, RT_OX). Radial plots denoting the peak oscillatory phases of (E) DEGs in shoots and (F) in roots estimated from the DIURNAL database (COL_LDHH condition). The expected counts are shown in gray, while peak phases are shown in pale orange for shoots and pale blue for roots. Numbers surrounding the outer periphery of the plots indicate the time in hours.

(G) Venn diagram showing the number of DEGs specific for shoots, for roots, and for the overlapped common DEGs (number in blue color).

(H–I) Relative RNA-seq expression analyses of (H) *YUC8* and (I) *PIF4* in shoots and roots. (H) and (I) share the same key.

(J–K) ChIP-qPCR analyses in shoots and roots showing CCA1 binding to target genes in (J) CCA1-ox and (K) CMG plants.

(L) GO-term enrichment analyses showing significantly enriched pathways of the DEGs common to shoots and roots.

(M and N) Relative RNA-seq expression analyses of (M) *BGLU6* and (N) *UMAMIT10* in shoots and roots.

(O) Venn diagrams showing the reduced overlap between DEGs in roots and genes related to the auxin signaling pathway in roots from previously published datasets.[44]

Data are presented as the mean + SD relative to the WT value of three independent biological experiments.

See also Figure S2.

Please cite this article in press as: Xiong et al., A circadian rheostat drives proton electrochemical gradients to optimize cell-type-specific growth in *Arabidopsis*, Cell (2026), https://doi.org/10.1016/j.cell.2025.12.056

evening-core clock genes such as *TOC1*, *elf3* (*EARLY FLOWERING 3*), or *LUX* (*LUX ARRHYTHMO*) were similarly expressed in shoots and roots (Figures S2E–S2I). Genes related to growth and light signaling, such as *HY5* and *HYH*, were downregulated in both CCA1-ox shoots and roots (Figures S2J and S2K). However, *hy5* mutants do not show a significant change in primary root length,[45] which suggests that changes in *HY5* expression are not responsible for the organ-specific phenotypes observed in CCA1-ox.

Root-specific DEGs (Figure 2G, DEGs RTs) included a variety of genes that were specifically repressed in CCA1-ox roots, such as genes related to cell wall loosening, for example, *EXPB2* (*EXPANSIN B2*) (Figure S2L), which is consistent with the reduced root growth. Some genes involved in glycosylation and carbohydrate metabolism, such as *BGLU6* (*BETA GLUCOSIDASE 6*), were significantly downregulated in CCA1-ox and upregulated in *cca1lhy* roots (Figure 2M). Root-specific DEGs included genes involved in the transport of metabolites across cellular membranes, such as *UMAMIT10* (*USUALLY MULTIPLE ACIDS MOVE IN AND OUT TRANSPORTERS 10*) (Figure 2N). Some of the DEGs (e.g., *GSTU11*, *GLUTATHIONE S-TRANSFERASE TAU 11*) were specifically expressed in roots (Figure S2M), or when expressed in shoots (*UGT73B1*, *UDP-GLUCOSYL TRANSFERASE 73B1*), they were not differentially expressed in CCA1-ox (Figure S2N). Our initial hypothesis was that the CCA1 root phenotypes might result from the differential effects of auxin in shoots and roots.[18] However, unlike in shoots, roots did not show widespread misregulation of the auxin signaling pathway, even when we compared root DEGs with datasets of auxin-related genes in roots[44] (Figure 2O). Thus, misregulation of auxin-related genes is unlikely to explain the observed root growth phenotypes.

CCA1 represses *SUC2* expression by directly binding to the *SUC2* promoter

Further data mining showed that the sucrose transporter *SUC2* was significantly downregulated in CCA1-ox and upregulated in the *cca1lhy* mutant (Figure 3A). *SUC2* appeared as DEGs in both shoots and roots with a log2-fold change of approximately −0.5 and −1.3, respectively. Other *SUC* genes were slightly but not significantly affected except for *SUC5* in shoots (Figures S3A–S3C). Thus, the altered shoot-to-root growth balance in CCA1 misexpressing plants could be due to inefficient phloem loading of photoassimilates. To explore this idea, we grew seedlings in media with increased sucrose concentrations as a way to reduce the sink strength and hence decrease the root dependence on shoots for growth.[43] Our results showed that sucrose progressively increased the root length of CCA1-ox seedlings: an evident increment compared with that observed in WT or *cca1lhy* roots (Figures S3D–S3F). The effect was particularly apparent when comparing root length in each genotype relative to its growth without sucrose (Figure 3B). Sucrose also increased *cca1lhy* root length but to a lesser extent than WT, particularly at higher dosages (Figures S3D, S3F, and S3G). Thus, the short root length of CCA1-ox plants can be rescued by sucrose, while its growth effect was reduced in *cca1lhy* roots. Similar sucrose-dependent root growth deficiency was reported for the *SUC2*[41] and for the sugar transporter *sweet11;12* mutants.[46] The results suggest that CCA1-ox roots are hypersensitive to sucrose-dependent growth, whereas *cca1lhy* are slightly hyposensitive compared with WT (Figures S3H–S3J). The sucrose growth effects in hypocotyls were reduced, and at certain sucrose concentrations, were nearly opposite to those observed in roots (Figures S3H–S3L).

Our results suggest that mis-expression of CCA1 affects the hypocotyl and root growth balance due to altered sucrose allocation. Consistently, the hypocotyl-to-root growth ratio in CCA1-ox seedlings was markedly dependent on the increasing sucrose concentrations (Figures 3C and 3D) due to the enhanced root growth (Figures S3D and S3E). In contrast, the ratio in the *cca1lhy* mutant remained largely unaffected regardless of sucrose concentration, showing overall a reduced ratio compared with WT (Figures 3C and 3E). The altered growth ratios closely correlated with sucrose content in roots, which was reduced in CCA1-ox but increased in *cca1lhy* (Figure 3F). Thus, transport to sink organs might be altered in CCA1-misexpressing plants. When sucrose transport is affected, transient carbohydrates accumulate in photosynthetic tissues.[41] Consistently, CCA1-ox shoots clearly accumulated more starch than WT and *cca1lhy* plants, indicating a shift toward carbohydrate storage rather than export (Figures 3G and S3M). Regulation of *SUC2* by CCA1 appears to be direct, since ChIP assays using CMG plants demonstrated CCA1 binding to the *SUC2* promoter (Figure 3H). Much lower enrichment was observed when amplifying the promoter of an unrelated gene or the transcriptionally inactive retrotransposon *TA3*, both used as negative controls (Figure 3H). Thus, CCA1 directly regulates *SUC2* expression by binding to its promoter.

The expression of ion transporters is tightly coordinated with the carbon status of the plant. Consistently, several key transporters known to be induced by sucrose were downregulated in CCA1-ox and upregulated in *cca1lhy* mutant seedlings (Figures 3I–3M). To verify that the organ-dependent growth phenotypes rely on CCA1 function repressing *SUC2* expression, we analyzed hypocotyl and root growth in plants overexpressing both *CCA1* and *SUC2* (SUC2-ox/CCA1-ox). Several lines with different ranges of *SUC2* overexpression were analyzed (Figures S3N and S3O). The short root growth of CCA1-ox seedlings was slightly but not fully rescued by overexpression of *SUC2* (Figures 3N and 3O). Previous studies have shown that SUC2-ox plants are stunted due to disrupted nutrient homeostasis in sink organs.[47] Thus, the reduced growth of SUC2-ox plants might explain the lack of restoration of CCA1-ox root length in the double SUC2-ox/CCA1-ox plants. Our results also suggest that CCA1 might regulate additional factors required for proper carbon allocation and root growth.

CCA1 controls proton electrochemical gradients in the apoplast of companion cells and impairs sucrose loading and transport velocity

CCA1 regulated the expression of the *Arabidopsis* H^+-pump ATPase *AHA3*, which was significantly downregulated in CCA1-ox and upregulated in *cca1lhy* (Figures 4A and 4B). This regulation is noteworthy as *AHA3* is expressed in the phloem[33,34,48] and is involved in sucrose loading and translocation to the sink tissues.[37,49] *AHA3* was expressed in both shoots and roots, although

Please cite this article in press as: Xiong et al., A circadian rheostat drives proton electrochemical gradients to optimize cell-type-specific growth in *Arabidopsis*, Cell (2026), https://doi.org/10.1016/j.cell.2025.12.056

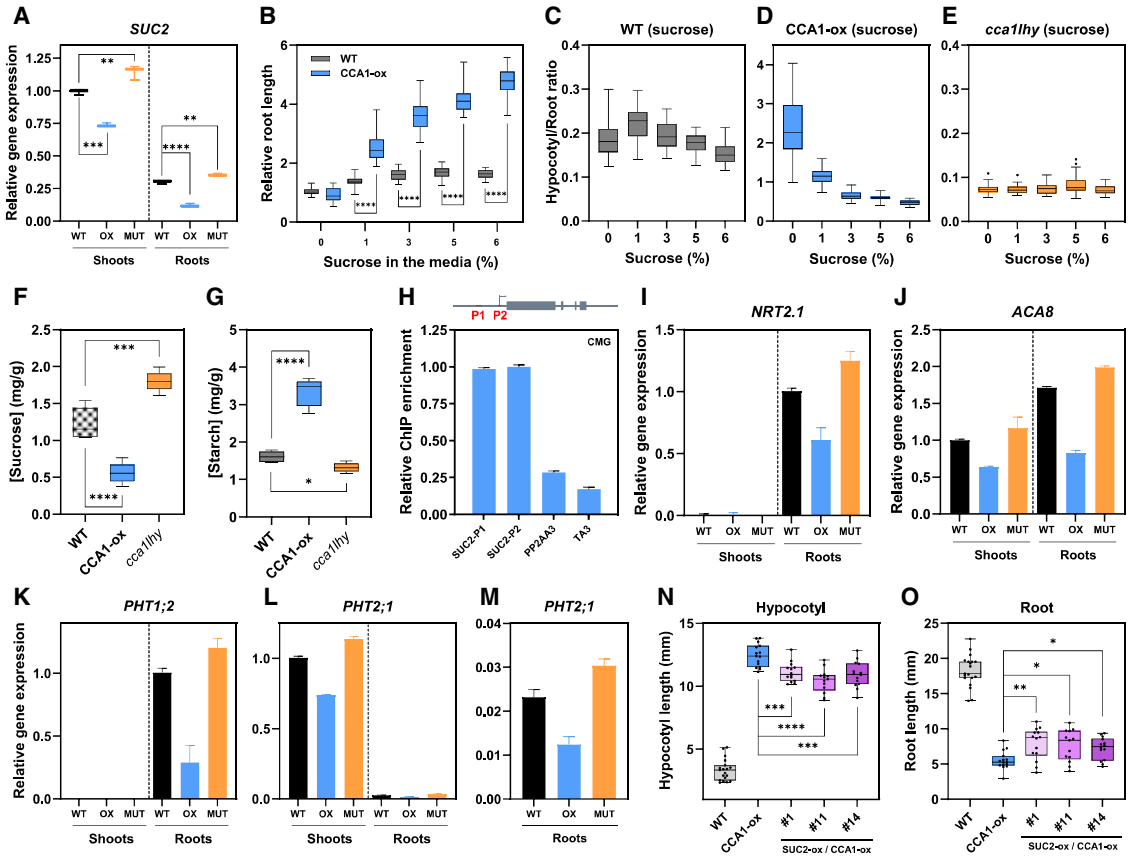

Figure 3. CCA1 represses *SUC2* expression by direct binding to the *SUC2* promoter

(A) Relative gene expression analysis by quantitative reverse-transcription PCR (RT-qPCR) of *SUC2* in WT, CCA1-ox, and *cca1lhy* shoots and roots. Gene expression is graphed relative to the WT shoot value.

(B) Relative root length of WT and CCA1-ox seedlings grown under LL at 15 μE light intensity with the indicated sucrose concentrations. Data are presented relative to the control (0% sucrose) for each genotype.

(C–E) Hypocotyl and root growth ratio of (C) WT, (D) CCA1-ox, and (E) *cca1lhy* seedlings grown under LL at 15 μE with varying sucrose concentrations.

(F) Sucrose concentration (mg/g of dry weight) analyzed by high-performance liquid chromatography (HPLC) in WT, CCA1-ox, and *cca1lhy* roots.

(G) Quantification of starch accumulation (mg/g of dry weight) measured by iodine staining in WT, CCA1-ox, and *cca1lhy* seedlings.

(H) ChIP analyses of CMG plants using two primer sets (*SUC2-P1* and *SUC2-P2*), whose positions are shown in the schematic diagram illustrating the genomic structure of *SUC2*.

(I–L) Relative gene expression analysis of (I) *NRT2,1*, (J) *ACA8*, (K) *PHT1;2*, and (L) *PHT2;1* in WT, CCA1-ox (OX), and *cca1lhy* (MUT) shoots and roots.

(M) *PHT2;1* expression in roots from (L) at an expanded scale. Gene expression is graphed as the mean + SD relative to the WT value of three independent biological experiments.

(N and O) (N) Hypocotyl and (O) root length in WT, CCA1-ox, and three SUC2-ox/CCA1-ox double over-expressing lines grown under LL at 15 μE light intensity. The boxplots display the median and interquartile range, with the whiskers extending to the data range (minimum to maximum). At least three biological replicates were performed per experiment. **** p value ≤ 0.0001; *** p value ≤ 0.001; ** p value ≤ 0.01; * p value ≤ 0.05.

See also Figure S3.

its expression was overall higher in shoots (Figure S4A). *AHA3* appeared in our RNA-seq dataset as a DEG in both shoots and roots with a log2-fold change of approximately −0.3. This change should be biologically quite relevant, as even subtle alterations of AHA3 can substantially affect the proton electrochemical gradient,[24] while *aha3* loss-of-function mutants are lethal.[32]

AHA3 is specifically expressed in companion cells[50] and acidifies the apoplast, establishing the proton motive force (ΔpH + ΔΨ) that drives SUC2-mediated sucrose/H^+ co-transport. Alkalinizing the apoplast reduces ΔpH and depolarizes the membrane, conditions known to diminish SUC2 activity, thereby limiting export from source leaves and lowering carbon supply to roots.[23,37,41,50] Time-course analyses over a diel cycle showed the rhythmic oscillation of *AHA3* expression and a downregulation in CCA1-ox plants at all time points examined (Figure 4C). To identify the relevance of CCA1 regulation of *AHA3* expression, we monitored *in vivo* phloem loading and transport activity using esculin, a fluorescent sucrose analog that is specifically loaded in the phloem by SUC2.[51] Our results showed that basipetal phloem velocity in roots was significantly reduced in CCA1-ox and increased in *cca1lhy* compared with WT (Figures 4D and 4E). The altered phloem transport velocity was not due to the elongated hypocotyls of CCA1-ox seedlings, as *elf3* and *elf4* mutants, which also exhibit long hypocotyls,

Please cite this article in press as: Xiong et al., A circadian rheostat drives proton electrochemical gradients to optimize cell-type-specific growth in *Arabidopsis*, Cell (2026), https://doi.org/10.1016/j.cell.2025.12.056

CellPress
OPEN ACCESS

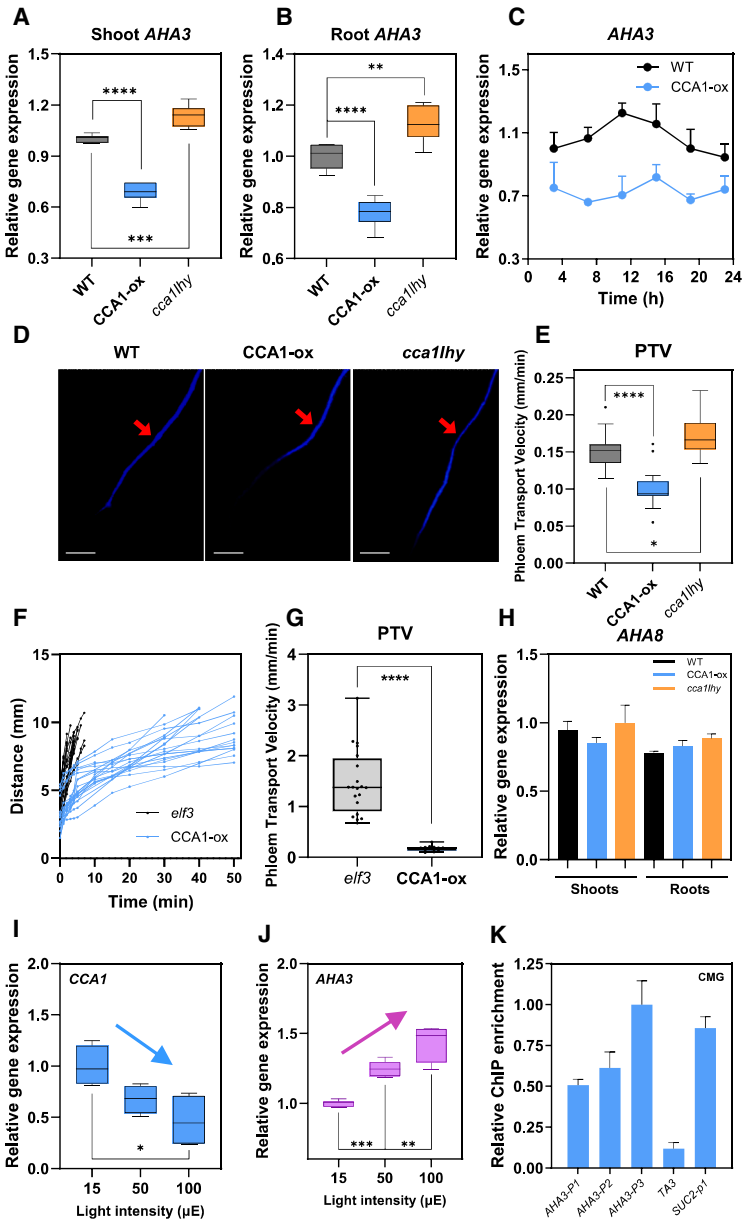

Figure 4. CCA1 controls proton electrochemical gradients in the apoplast of companion cells and impairs sucrose loading and transport velocity

(A and B) Relative gene expression analysis by RT-qPCR of *AHA3* in WT, CCA1-ox, and *cca1lhy* in (A) shoots and (B) roots.

(C) Time-course analysis under LD cycles of *AHA3* expression in WT and CCA1-ox. Gene expression is graphed as the mean + SD relative to the WT value at ZT3.

(D) Stereomicroscope images of esculin transport in WT, CCA1-ox, and *cca1lhy* roots imaged in plants grown under LL conditions without previous entrainment to exclude the effects of differential circadian timing phenotypes. Arrowheads indicate the first position of the visible esculin. Scale bar, 0.5 mm.

(E) Phloem transport velocity (PTV) of esculin along the phloem of WT, CCA1-ox, and *cca1lhy* roots.

(F and G) (F) Traveled distance of esculin along the phloem and (G) PTV in the hypocotyl of *elf3* and CCA1-ox.

(H) Relative RNA-seq gene expression analysis of *AHA8* in WT, CCA1-ox, and *cca1lhy* shoots and roots. Gene expression is graphed as the mean + SD relative to the WT value.

(I and J) Relative gene expression analysis by RT-qPCR of (I) *CCA1* and (J) *AHA3* in WT plants at the indicated light intensities. Gene expression is graphed relative to the 15 μE value. Arrows in (I) and (J) denote the ascending or descending trend.

(K) ChIP analyses of CMG plants showing CCA1 binding to the *AHA3* promoter using three primer sets.

The boxplots display the median and interquartile range, with the whiskers extending to the data range (minimum to maximum). Three independent biological replicates were performed per experiment. **** p value $\leq$ 0.0001; *** p value $\leq$ 0.001; ** p value $\leq$ 0.01; * p value $\leq$ 0.05.

See also Figure S4.

showed a significantly increased phloem transport velocity (Figures 4F, 4G, S4D, and S4E).

Regulation of *AHA3* by CCA1 may represent a critical bottleneck for sucrose export due to the slower transport rate of proton pumps compared with sucrose transporters like SUC2. The expression of other *AHA* genes proposed to be expressed in phloem companion cells was not significantly misregulated in CCA1-ox or *cca1lhy* relative to the WT (Figures 4H, S4B, and S4C). The inverse regulatory relationship between CCA1 and AHA3 was also evident in response to light, where increasing light intensity suppressed *CCA1* expression but induced *AHA3* (Figures 4I and 4J). Similar inverse gene expression correlation in response to light was observed in CMG plants (Figures S4F–S4H). Our ChIP assays using CMG plants confirmed the binding of CCA1 to the *AHA3* promoter, to a similar degree to that observed for *SUC2* (Figures 4K and S4I). Thus, CCA1 directly regulates *AHA3* expression by binding to its promoter. *AHA3* expression was still downregulated in the double SUC2-ox/CCA1-ox plants (Figure S4J), which explains the lack of root length restoration in the double SUC2-ox/CCA1-ox lines.

Opposing roles of CCA1 regulating proton electrochemical signals in the apoplast of epidermal cells and in the phloem

If CCA1 regulates *AHA3*, changes in the proton electrochemical gradient should be evident in the apoplast of companion cells in CCA1-ox plants. Monitoring pH in highly acidic environments is technically challenging, especially in the phloem. Thus, we used plants expressing a genetically encoded plasma membrane-anchored pH sensor (PM-Apo-Acidin4).[52] To provide cell-type specificity, we also expressed the pH sensor under the *Commelina yellow mottle virus* (*CoYMV*) promoter, which drives companion-cell-specific expression.[47,53,54] Microscopy imaging revealed specific fluorescence signals in the apoplasts of companion cells in hypocotyls (Figures 5A and S5A) and in roots (Figures 5B and S5B). Ratiometric analyses to compute the pH differences in the apoplast showed that the apoplastic pH of CCA1-ox plants was significantly higher than in WT in both hypocotyls and roots (Figures 5A and 5B). Similar results were obtained in roots of plants constitutively expressing the pH sensor

Please cite this article in press as: Xiong et al., A circadian rheostat drives proton electrochemical gradients to optimize cell-type-specific growth in *Arabidopsis*, Cell (2026), https://doi.org/10.1016/j.cell.2025.12.056

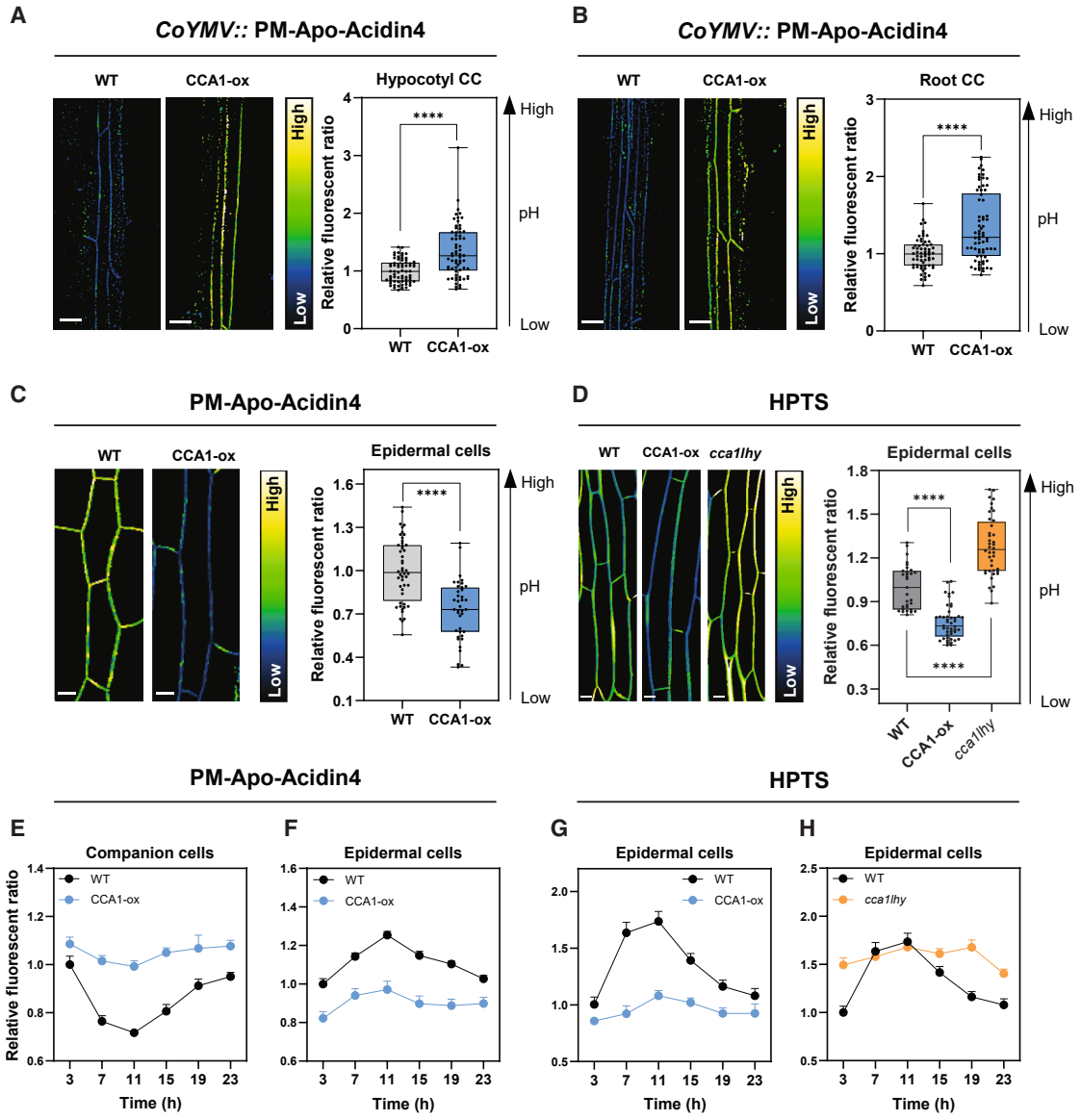

Figure 5. Opposing roles of CCA1 regulating proton electrochemical signals in the apoplast of epidermal cells and in the phloem

(A and B) Confocal images and ratiometric quantification of (A) relative apoplastic pH in hypocotyl phloem companion cells using the *CoYMV::*PM-Apo-Acidin4 pH sensor in WT and CCA1-ox seedlings and (B) relative apoplastic pH in root phloem companion cells using the *CoYMV::*PM-Apo-Acidin4 pH sensor in WT and CCA1-ox seedlings.

(C) Relative apoplastic pH in hypocotyl epidermal cells using PM-Apo-Acidin4 in WT and CCA1-ox seedlings.

(D) Relative apoplastic pH in hypocotyl epidermal cells by HPTS staining.

(E–H) Diel time-course ratiometric analyses of (E) apoplastic pH in WT and CCA1-ox hypocotyl companion cells using *CoYMV*::PM-Apo-Acidin4 pH sensor, (F) apoplastic pH in WT and CCA1-ox hypocotyl epidermal cells using PM-Apo-Acidin4 pH sensor, (G) apoplastic pH in WT and CCA1-ox hypocotyl epidermal cells using HPTS staining, and (H) apoplastic pH in WT and *cca1lhy* hypocotyl epidermal cells using HPTS staining.

Data are shown as the mean + SD. The boxplots display the median and interquartile range, with the whiskers extending to the data range (minimum to maximum). Three independent biological replicates were performed per experiment. **** p value $\leq$ 0.0001. Scale bars, 10 μm.

See also Figure S5.

(Figure S5C). Thus, the enhanced local apoplastic alkalinization in the phloem correlates with the reduced *AHA3* expression in CCA1-ox plants.

As auxin acidifies the apoplast of epidermal cells in shoots[19,21] and CCA1 promotes auxin signaling and hypocotyl growth, we examined whether the apoplastic pH of hypocotyl epidermal cells was affected in CCA1-ox plants. Using the constitutively expressed pH sensor, we found an increased apoplastic acidification in CCA1-ox compared with WT (Figures 5C and S5D). The opposite regulation of apoplastic

pH by CCA1 in the phloem and in hypocotyl epidermal cells was further supported by using a pH-sensitive dye (8-hydroxypyrene-1,3,6-trisulfonic acid trisodium salt, HPTS), which revealed reduced and increased apoplastic pH of CCA1-ox and *cca1lhy* hypocotyl epidermal cells, respectively (Figures 5D and S5E).

Time-course analyses over a diel cycle also revealed a rhythmic oscillation of the apoplastic pH in the phloem of WT hypocotyls (Figure 5E) and roots (Figure S5F), with higher pH values in CCA1-ox plants at all time points examined. The apoplastic pH in epidermal cells of WT hypocotyls also oscillated rhythmically in a nearly antiphasic manner relative to the rhythmicity of the pH in the phloem. Consistently, epidermal apoplastic pH was reduced throughout the time course in CCA1-ox plants (Figure 5F). HPTS staining of hypocotyls also confirmed these patterns, showing reduced pH in the epidermal cells of CCA1-ox plants (Figure 5G) and elevated pH in *cca1lhy* mutants compared with WT (Figure 5H). The contrasting and cell-type-specific effects on apoplastic pH are consistent with the hypocotyl and root growth phenotypes observed in seedlings misexpressing CCA1.

To confirm the triad CCA1, apoplastic pH in the phloem, and root growth, we generated plants expressing CCA1-YFP specifically in companion cells. To that end, we expressed CCA1 under the *CoYMV* promoter[47] in the *cca1lhy* background (Figures 6A and S6A). CCA1 companion-cell-specific expression was sufficient to significantly shorten the long roots of *cca1lhy* plants (Figure 6B), while hypocotyl length was not manifestly altered (Figure 6C). Therefore, *CCA1* expression just in the vasculature can reduce root growth. If CCA1 regulation of root growth relies on *AHA3* repression, then overexpressing *AHA3* in the CCA1-ox background should restore the root growth. Analyses of AHA3-ox/CCA1-ox double-expressing plants (Figures S6B–S6D) showed that AHA3 overexpression indeed reverted the reduced root growth of CCA1-ox plants (Figures 6D and 6E) without altering the long hypocotyl (Figure 6F). Esculin analysis revealed that the reduced basipetal phloem transport velocity observed in CCA1-ox plants was also rescued by overexpressing AHA3 (Figures 6G and S6E). Thus, an important determinant of CCA1 regulation of sucrose export to sink tissues is the repression of *AHA3* expression. The use of the companion-cell-specific pH sensor showed that the CCA1-ox pH was restored to nearly WT values by overexpressing AHA3 (Figure 6H). The observed pH changes do not pervade all cell types, as HPTS staining showed that the apoplastic pH in epidermal cells was not significantly different in CCA1-ox and AHA3-ox/CCA1-ox plants (Figure S6F). Thus, restoration of the pH was specific to the apoplast of companion cells. Consistently, analyses of single AHA3 overexpressing plants in the WT background (Figure S6G) significantly increased the length of roots (Figure 6I) but not of hypocotyls (Figure S6H).

The function of CCA1 on root growth was mathematically modeled through integrated analyses of sucrose dynamics in shoots, phloem loading rate, and root growth[55] (Figure 6J). Computational simulations of the root growth patterns (Figures 6K and 6L) revealed that sucrose loading rates into the phloem were approximately 50% lower in CCA1-ox compared with WT, while the *cca1lhy* mutant showed about 115% increase in loading rates. Our experimental and mathematical analyses confirm that CCA1-mediated repression of *AHA3* specifically in the phloem alters the proton electrochemical gradient, thereby affecting sucrose loading and transport to roots and ultimately modulating root elongation and shoot-to-root growth balance. The results explain why overexpressing SUC2 in CCA1-ox failed to fully restore the CCA1-ox root length. The reduced expression of *AHA3* compromises the proton electrochemical gradients necessary for efficient sucrose loading. The opposing regulation of proton electrochemical signals in epidermal cells and in the phloem accounts for the dual role of CCA1 promoting hypocotyl growth while inhibiting root elongation.

DISCUSSION

The connection between CCA1 and hypocotyl growth has been previously established,[8–10] but here, we found that CCA1 misexpressing plants display opposite growth phenotypes in hypocotyls and roots. Although the plants still respond to different light fluences, the phenotypes appear more pronounced under low light intensity, potentially due to limited sucrose availability for export. During skotomorphogenesis, shoot growth is prioritized over root growth, while adding exogenous sucrose mitigates the dark-induced inhibition of root growth.[56] The CCA1-ox phenotypes partially resemble growth during skotomorphogenesis. Although CCA1-ox roots grown in the light are not as short as those grown in darkness, the shoot-root growth ratio in CCA1-ox plants is clearly skewed toward shoot growth. Shoots and roots are dynamically interconnected, and the circadian function is modulated by this connection.[57] For example, the shoot apex influences rhythms in roots[58] through photosynthetic signals[59] and by the temperature-dependent movement of the clock protein ELF4 from shoots to roots.[60] Light perception in shoots can also generate rhythms in root hairs.[13]

CCA1 and LHY function as partially redundant transcription factors.[61,62] CCA1-ox plants show pronounced growth phenotypes that are opposite to those observed in the *cca1lhy* mutant. Given that *LHY* expression is strongly repressed in CCA1-ox plants, the observed phenotypes indicate that CCA1 can regulate growth even when *LHY* activity is nearly abolished. Early studies suggested that ELF3 acts downstream of CCA1, mediating the repression of *PIF4* and *PIF5* in the control of hypocotyl elongation.[63] Later studies demonstrated that CCA1 controls hypocotyl growth by directly binding the *PIF4* promoter to activate the auxin pathway.[8,9] CCA1 interacts additively with other members of the single-MYB transcription factor family in the control of growth.[64] These proteins also repress hypocotyl elongation in a daylength- and sucrose-dependent manner by a mechanism that depends on the regulation of *PIF4* and *PIF5* expression.[65] Here, we found that *PIF4* expression and CCA1 binding to the *PIF4* promoter were significantly reduced in roots, supporting the existence of organ-specific regulatory mechanisms. The results also resemble previous studies demonstrating the organ-specific role of PIF4 regulating temperature responses in above-ground tissues.[45]

The acid growth theory posits that auxin-induced apoplast acidification promotes cell wall loosening, thereby facilitating cell elongation.[15,66] The mechanism involves receptor-like

Please cite this article in press as: Xiong et al., A circadian rheostat drives proton electrochemical gradients to optimize cell-type-specific growth in *Arabidopsis*, Cell (2026), https://doi.org/10.1016/j.cell.2025.12.056

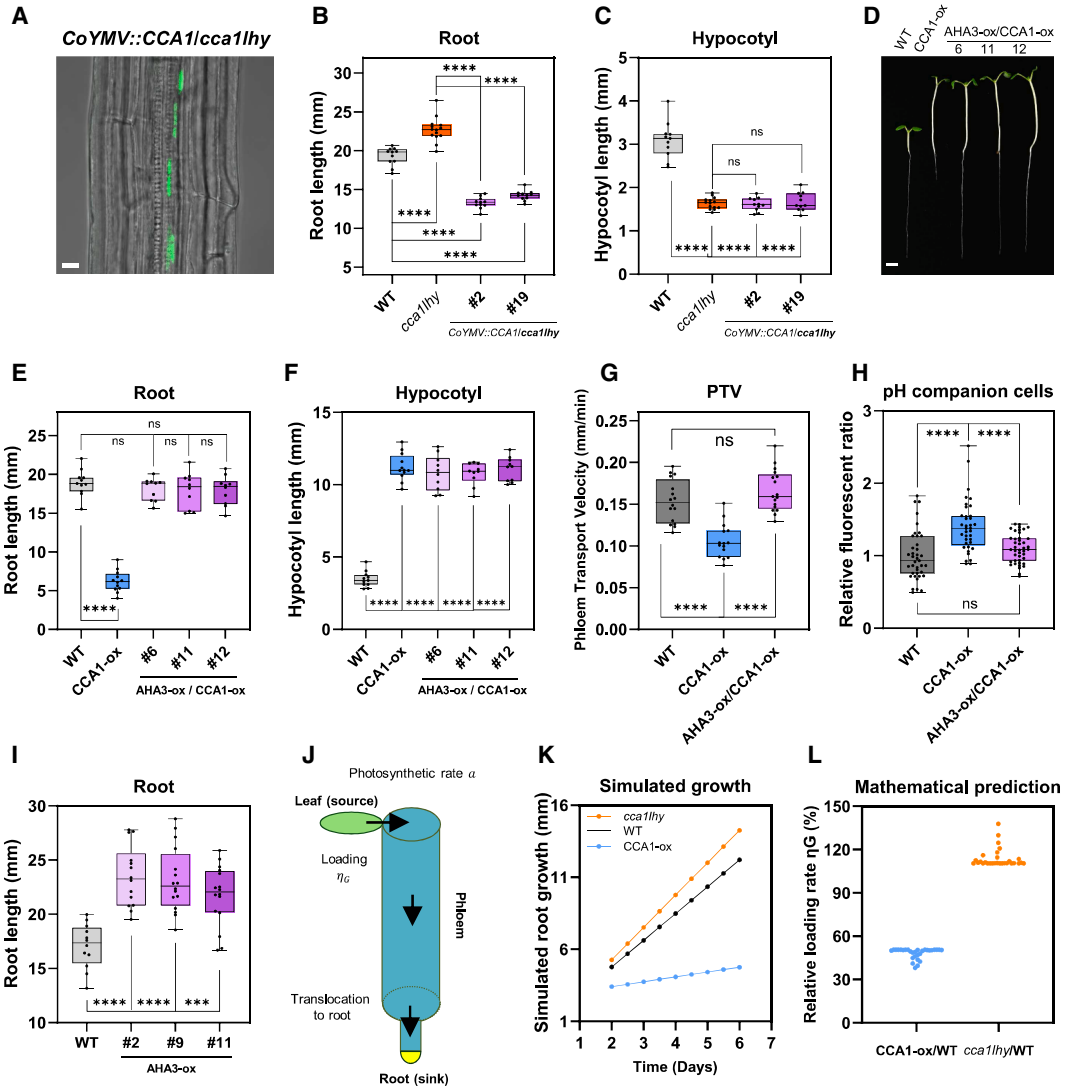

Figure 6. Restoration of growth by specific expression of CCA1 in companion cells and by overexpression of AHA3 in CCA1-ox plants

(A) Specific localization of CCA1 in the root vasculature of plants expressing *CoYMV::CCA1-YFP* in a *cca1lhy* mutant background. Scale bar, 10 μm.

(B) Root length in WT, *cca1lhy*, and two *CoYMV::CCA1-YFP/cca1lhy* lines grown under LL at 15 μE light intensity.

(C) Hypocotyl length in WT, *cca1lhy*, and two *CoYMV::CCA1-YFP/cca1lhy* lines grown under LL at 15 μE light intensity.

(D) Representative image of WT, CCA1-ox, and the three AHA3-ox/CCA1-ox lines. Scale bar, 2 mm.

(E and F) (E) Root and (F) hypocotyl length in WT, CCA1-ox, and three AHA3-ox/CCA1-ox lines grown under LL at 15 μE light intensity.

(G) PTV of esculin along the root phloem of WT, CCA1-ox, and AHA3-ox/CCA1-ox (line #6) roots.

(H) Quantification of the relative apoplastic pH in hypocotyl companion cells assayed with *CoYMV::PM-Apo-Acidin4*.

(I) Root length in WT and three AHA3-ox lines grown under LL at 15 μE light intensity.

(J) Schematic drawing for estimation of sucrose loading rates using the phloem sucrose transport model.

(K and L) (K) Simulated root growth (corresponding to the data in Figures 1I and 1J), and (L) predicted sucrose loading rates of CCA1-ox and *cca1lhy* relative to WT using a mathematical model that integrates sucrose dynamics in shoots, sucrose loading, and root growth. A range of values for the photosynthetic rate parameter (a) from 0.01 to 0.3 was used for model fitting.

The boxplots display the median and interquartile range, with the whiskers extending to the data range (minimum to maximum). Three independent biological replicates were performed per experiment. **** p value $\leq$ 0.0001; *** p value $\leq$ 0.001; ns, no significant difference.

See also Figure S6.

transmembrane kinases that ultimately activate proton ATPases. Our results are consistent with the acid growth theory, showing that CCA1 misexpressing seedlings alter the apoplastic pH of epidermal cells in hypocotyls. The RNA-seq analysis in shoots revealed the upregulation of many SAUR (SMALL AUXIN-UP RNA) genes. The SAUR proteins activate the plasma membrane H^+-ATPases, leading to the acidification of the apoplast in hypocotyl epidermal cells.[67] Notably, light-grown hypocotyls exhibit a

higher apoplastic pH, which can counteract auxin-induced over-acidification.[21] The results open the possibility that CCA1 operates at the intersection of light and auxin signaling pathways to modulate the apoplastic pH in epidermal cells. The phloem apoplast alkalinization by CCA1-ox disrupts sucrose export and consequently inhibits root growth. The increased apoplastic pH specifically in the phloem suggests a safeguard mechanism, limiting sucrose export to ensure sufficient resources for shoot growth. Thus, by balancing the apoplastic pH in epidermal cells and in the phloem, CCA1 may control hypocotyl and root growth.

The circadian clock controls carbon assimilation[68] and the rhythmic flux of carbon into sugars.[69] In turn, sugars provide feedback to regulate the clock.[70–72] PRR7 is the core clock component responsible for the photosynthetic entrainment of the circadian clock[67,70] and regulation of nutrient transport,[14] while the sugar-responsive circadian regulator bZIP63 (BASIC LEUCINE ZIPPER 63) up-regulates *PRR7* under low-light conditions with low endogenous sugar.[67] Changes in *CCA1* transcription to sugars depend on *PRR7* dynamics,[70] although mutant plants of bZIP63 impair growth under light-dark cycles, but not under constant light,[73] which are the conditions that we used in our assays. Here, we focused on CCA1 regulating resource allocation and root growth. Efficient phloem transport of sucrose from shoot to root is crucial for root growth.[38,42] Sucrose dynamically accumulates in the phloem, ensuring the proper balance of source export with sink demand. *SUC2* is expressed in companion cells,[41] and *SUC2* mutants show significantly shorter roots compared with WT.[42] Adding sucrose, which reduces root dependence on shoots,[43] rescued the root growth phenotype of CCA1-ox plants. SUC2 activity is controlled by a complex network of cues and signaling pathways, including, among many others, light and diurnal cycles.[38] Analyses of publicly available datasets (DIURNAL) show that *SUC2* expression oscillates rhythmically under diel cycles, with a trough around dawn, coinciding with the time of *CCA1* peak expression. This timing is consistent with CCA1 repressing *SUC2* expression. *SUC2* appeared misregulated in both shoots and roots. While SUC2's role in sucrose loading in shoots is well established, its potential function in roots remains less well understood.

Although CCA1 directly binds to the *SUC2* promoter, overexpressing SUC2 in CCA1-ox plants only partially rescued the root growth phenotype. SUC2-ox plants are stunted due to disrupted nutrient homeostasis in sink organs.[47] Additional factors, such as members of the SWEET transporters, might also contribute to the observed phenotypes, as some of these genes, particularly *SWEET13*, appeared downregulated in our RNA-seq. However, *SWEET13*, as well as *SWEET11* and *SWEET12*, are expressed in the phloem parenchyma, while expressing *CCA1* specifically in companion cells is sufficient to inhibit root elongation. It would also be interesting to check possible changes in the role of CCA1 as the plant develops and the source-sink relationship becomes more complex and dynamic. Further, CCA1 may integrate responses to environmental stresses that require extra carbon allocation for root growth. The root growth rate of the ecotype Ws-2 was found to be comparable to that of the *cca1lhy* double mutant, while the mutant showed reduced growth during the late night.[74] The divergence might be due to the different ecotypes used in both studies. It is also interesting that in *Brassica rapa*, there is evidence that rapidly elongating hypocotyls are sink organs, not sources, and experiments with *Arabidopsis* mutants also support this notion.[75] Thus, the rapidly growing hypocotyl of CCA1-ox might not be a carbon source. Since the CCA1-ox hypocotyls are clearly elongated, our results suggest that the activated auxin pathway in shoots overrides the possible sink nature of hypocotyls. This idea is supported by the acidic pH of the apoplast of epidermal cells in CCA1-ox hypocotyls. Similarly, the long hypocotyls of CCA1-ox suggest that the auxin signaling pathway overcomes the low *SUC2* expression in shoots. We propose that the reduction of sucrose export in CCA1-ox plants leads to higher starch accumulation in shoots, which agrees with previous studies showing that downregulation of sucrose loading and transport results in higher starch content in the mature leaves. The results are also in line with previous studies showing that *cca1lhy* mutant plants accumulate less starch and show premature depletion of starch reserves.[76,77] It is also possible that the over-accumulation of starch could stem from regulation of metabolic pathways. Since CCA1-ox plants are morning-locked,[78] this might favor daytime metabolic processes (e.g., starch synthesis) and prevent nighttime processes (e.g., starch degradation).

In the vegetative tissues of adult *Arabidopsis* plants, AHA1 and AHA2 account for up to 80% of the ATPase activity. Despite this, single *aha1* or *aha2* mutants remain viable,[24] whereas *aha3* mutants are lethal.[32] AHA3 alters the electric potential and pH gradient required for phloem loading and transport of solutes.[23] Our studies focused on early stages of seedling development, a time when AHA3 may play a crucial role in regulating photoassimilate partitioning. Apoplastic pH and membrane potential are restricted within narrow limits,[24] providing sufficient protons for co-transport without creating thermodynamic constraints on proton pump activity.[79] Even small changes in AHA3 activity can importantly impact the proton electrochemical gradient.[24] For example, a shift of just half a pH unit triggers cell elongation in the transition zone of roots.[52] Not surprisingly, companion cells of apoplasmic loaders exhibit high proton pump ATPase expression and an increased proton motive force compared with surrounding phloem parenchyma cells.[80] Consequently, altered AHA3 function impairs the mobilization of resources to sink organs, affecting growth, storage, metabolism, and nutrient uptake.[36,81–84]

Given its essential role, AHA3 expression and activity must be tightly regulated. While several environmental factors are known to influence AHA activity at the transcriptional level,[25] less is known about upstream transcription factors that directly regulate *AHA* expression. Here, we identify CCA1 as a key regulator of *AHA3* and demonstrate that it directly binds to the *AHA3* promoter to control its expression. The results are not solely based on CCA1 overexpression but also on the analyses of *cca1lhy* mutant plants that show upregulation of *AHA3* expression. Sucrose accumulation may also activate AHA3 activity in companion cells, while light in mesophyll cells induces hyperpolarization of the plasma membrane through activation of proton pump ATPases.[85] AHA3 activation may require a threshold of sucrose accumulation. A concentration threshold of photosynthetic-derived sugars also contributes to clock entrainment, in a process mediated by PRR7 acting through CCA1,[70] while the

Please cite this article in press as: Xiong et al., A circadian rheostat drives proton electrochemical gradients to optimize cell-type-specific growth in *Arabidopsis*, Cell (2026), https://doi.org/10.1016/j.cell.2025.12.056

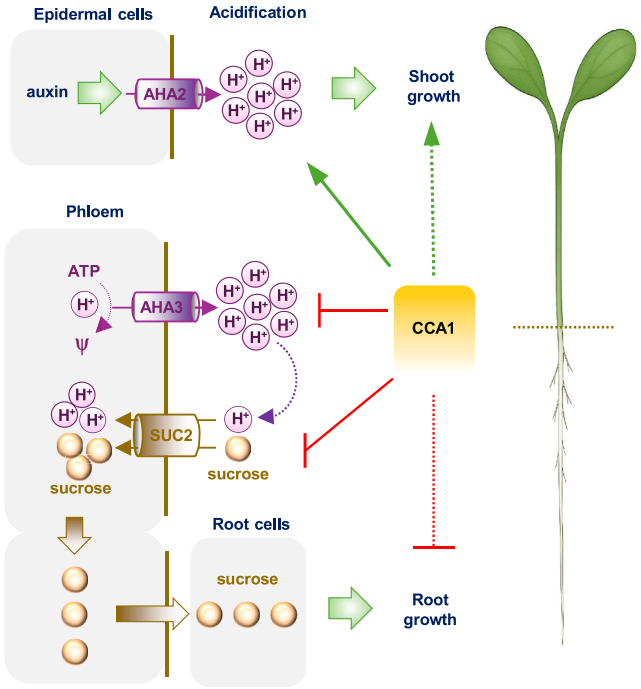

Figure 7. Schematic model depicting the CCA1-mediated differential regulation of hypocotyl and root growth

The model illustrates CCA1 opposing modulation of apoplastic pH in epidermal cells and phloem companion cells, leading to contrasting effects on growth. In epidermal cells, CCA1 promotes hypocotyl growth by activating auxin signaling, which stimulates plasma membrane H⁺-ATPases and acidifies the apoplast. In phloem companion cells, CCA1 increases the apoplastic pH by repressing *AHA3* and *SUC2*, modulating sucrose distribution and root growth. AHA proton pumps are shown as purple cylinders, SUC2 as a brown cylinder, protons as purple circles, and sucrose as brown spheres. Green arrows indicate activation, while red lines ending in perpendicular bars represent repression.

clock-related component GIGANTEA (GI) influences the sucrose-dependent changes on rhythmicity of the shoot clock.[72] Thresholds also govern apoplastic pH regulation. For instance, epidermal apoplast acidification promotes growth only within a specific pH range, as excessive acidification below a critical threshold inhibits elongation.[21]

aha mutants attenuate touch responses and show a reduced growth rate.[27] In WT plants, mechano-stimulated electrical signals were undetectable in the early morning and appeared only at midday.[27] The absence of these signals coincides with the peak of *CCA1* expression and with the *AHA3* repression by *CCA1*. This temporal regulation suggests that CCA1 might contribute to touch-stimulated leaf movements observed in plants like *Mimosa pudica*, where such movements peak around midday.[27] Further studies could also investigate regulatory mechanisms beyond transcriptional control, given that AHAs are also subject to post-translational regulation.[22] Further, it is possible that phloem-enriched modulators of AHA3 might be specifically expressed in the phloem but absent in the epidermis. Thus, constitutive expression of AHA3 does not alter the pH in hypocotyl epidermal cells or hypocotyl growth. Nevertheless, our analyses of double AHA3-ox/CCA1-ox plants revealed that AHA3-ox rescued the short root phenotype observed in CCA1-ox. The findings underscore the complex interplay between transcriptional and post-translational mechanisms in regulating AHA3 function.

CCA1 mis-expression disrupts the rhythmic regulation of apoplastic pH in both phloem and epidermal tissues, leading to altered pH amplitudes. These changes in apoplastic pH are likely to contribute to the aberrant hypocotyl and root growth phenotypes observed in CCA1-ox and *cca1lhy* seedlings, highlighting a previously underappreciated link between the circadian clock and pH-mediated growth regulation. The mechanism by which CCA1 promotes acidification in the apoplast of epidermal cells could be related to the CCA1 activation of auxin signaling. Auxin can activate plasma membrane H⁺-ATPases, resulting in apoplastic acidification and promotion of cell expansion.[19,21] This mechanism provides a plausible explanation for the changes in epidermal apoplast acidification observed in CCA1-ox and *cca1lhy*. The mechanism of AHA action has been described.[23,37,41] Apoplastic alkalinization reduces ΔpH and depolarizes the membrane, conditions known to impair SUC2 activity, thereby limiting sucrose export from source leaves and decreasing carbon supply to the roots. By repressing *AHA3* expression, CCA1 controls sucrose export to sink tissues. Regulation of *AHA3* by CCA1 could represent an important checkpoint for sucrose export, especially considering that the transport speed of proton pump ATPases is relatively slow compared with carriers such as SUC2.[86] Our results explain why SUC2-ox cannot rescue the root growth phenotype of CCA1-ox, as SUC2 overexpression cannot overcome the altered proton electrochemical gradients resulting from the reduced expression of *AHA3* in SUC2-ox/CCA1-ox plants. AHA3 function in roots might also be important for sucrose transport and unloading, as a proper proton motive force is required for effective sugar transport and import into sink cells.[87–89]

We propose that CCA1 functions as a molecular rheostat, fine-tuning proton electrochemical signals to optimize carbon allocation and ensure sufficient resources for sustaining growth and metabolism in source tissues (Figure 7). Misexpression of CCA1 disrupts this balance, affecting photoassimilate distribution to sink tissues. Thus, CCA1 performs a dual function: promoting hypocotyl growth by activating auxin signaling and acidifying the apoplast of epidermal cells while increasing the pH in the apoplast of companion cells, regulating sucrose distribution through repression of *SUC2* and *AHA3* expression (Figure 7). The circadian regulation of AHA3 might be important for coordinating growth with daily energy availability. In the early morning, when photosynthetic activity and energy supply are still low, CCA1 might act as a rheostat to maintain sucrose allocation toward shoots, supporting continued growth and energy production. As the day progresses and photosynthesis increases, sucrose becomes more abundant, allowing enhanced transport toward roots. Thus, circadian control of the proton pump might help optimize phloem loading and sucrose distribution between shoots and roots in response to the plant's daily metabolic status, ultimately contributing to coordinated growth and energy balance. This mechanism is also consistent with the more pronounced growth phenotypes under low-light conditions, when

energy production is limited and a precise temporal regulation of sucrose partitioning becomes even more critical for sustaining balanced shoot and root growth. CCA1 may also contribute to energy conservation, as maintaining the proton motive force in companion cells demands substantial ATP consumption.

Limitations of the study

We did not investigate the molecular mechanisms by which CCA1 regulates apoplastic pH in epidermal cells. This regulation may occur indirectly through activation of the auxin signaling pathway, although a more direct role cannot be excluded. Future studies could address the potential direct regulation, for instance, by examining whether CCA1 functions at the intersection of light and auxin signaling to modulate apoplastic pH in epidermal cells. It would also be interesting to elucidate the molecular basis underlying the lack of CCA1 binding to the *PIF4* promoter in roots. Moreover, future work could explore a possible role of AHA3 in sucrose unloading in sink tissues. Methodologically, measuring pH in the phloem sap was not feasible under our growing conditions. The development of novel techniques with a proper signal-to-noise ratio could enable such analyses in the future.

RESOURCE AVAILABILITY

Lead contact

Further information and requests for resources and reagents should be directed to and will be fulfilled by the lead contact, Paloma Mas (paloma.mas@cragenomica.es).

Materials availability

All materials generated in this study are available upon request and should be directed to the lead contact, Paloma Mas.

Data and code availability

- RNA-seq data is available at Mendeley Data: http://www.doi.org/10.17632/3jgj3b365r.1 and at GEO: GSE315134.
- Microscopy data reported in this paper will be shared by the lead contact upon request.
- The source code for the mathematical modeling is available at GitHub: https://github.com/seki-design/sucrose-transport.
- Any additional information required to reanalyze the data reported in this paper is available from the lead contact upon request.

ACKNOWLEDGMENTS

We thank Prof. T. Schmülling (Institute of Biology/Applied Genetics, Berlin, Germany) for providing the *cca1lhy* double-mutant seeds, Prof. B.G. Ayre (University of North Texas, USA) for the *pGPTV-CoYMVp::CmR-ccdB* vector, and Prof. N. Paris (IPSiM, Univ Montpellier, France) for the PM-Apo-Acidin4 seeds and vectors. The Mas laboratory is funded with research grant PID2022-137770NB-I00 from MCIU/AEI/10.13039/501100011033 and "ERDF/EU," from the Ramon Areces Foundation, as well as through the SGR Program (2021-SGR-01131) funded by the Secretaria d'Universitats i Recerca del Departament d'Empresa i Coneixement de la Generalitat de Catalunya (AGAUR). The Mas laboratory acknowledges financial support from grants SEV-2015-0533 and CEX2019-000902-S funded by MICIU/AEI/10.13039/501100011033 and by the CERCA Programme/Generalitat de Catalunya. L.X. was a recipient of a CSC fellowship funded by the China Scholarship Council.

AUTHOR CONTRIBUTIONS

Conceptualization, P.M.; methodology, L.X.; mathematical modeling, M.S. and A.S.; writing—original draft, P.M.; writing—review & editing, L.X., M.S., A.S., and P.M.; funding acquisition, M.S., A.S., and P.M.; supervision, P.M.

DECLARATION OF INTERESTS

The authors declare no competing interests.

STAR★METHODS

Detailed methods are provided in the online version of this paper and include the following:

- KEY RESOURCES TABLE
- EXPERIMENTAL MODEL AND STUDY PARTICIPANT DETAILS
  - Plant material and growing conditions
- METHOD DETAILS
  - Hypocotyl and root length measurements
  - RNA-seq analysis
  - Phloem transport velocity
  - Gene expression analysis by RT-qPCR
  - Chromatin immunoprecipitation assays
  - Analyses of sucrose content and starch accumulation
  - Mathematical modelling
- QUANTIFICATION AND STATISTICAL ANALYSIS

SUPPLEMENTAL INFORMATION

Supplemental information can be found online at https://doi.org/10.1016/j.cell.2025.12.056.

Received: July 7, 2025
Revised: November 6, 2025
Accepted: December 30, 2025

REFERENCES

1. Dowson-Day, M.J., and Millar, A.J. (1999). Circadian dysfunction causes aberrant hypocotyl elongation patterns in Arabidopsis. Plant J. *17*, 63–71. https://doi.org/10.1046/j.1365-313X.1999.00353.x.
2. Nozue, K., Covington, M.F., Duek, P.D., Lorrain, S., Fankhauser, C., Harmer, S.L., and Maloof, J.N. (2007). Rhythmic growth explained by coincidence between internal and external cues. Nature *448*, 358–361. https://doi.org/10.1038/nature05946.
3. Nusinow, D.A., Helfer, A., Hamilton, E.E., King, J.J., Imaizumi, T., Schultz, T.F., Farré, E.M., and Kay, S.A. (2011). The ELF4-ELF3-LUX complex links the circadian clock to diurnal control of hypocotyl growth. Nature *475*, 398–402. https://doi.org/10.1038/nature10182.
4. Covington, M.F., and Harmer, S.L. (2007). The circadian clock regulates auxin signaling and responses in Arabidopsis. PLoS Biol. *5*, e222. https://doi.org/10.1371/journal.pbio.0050222.
5. Paik, I., Kathare, P.K., Kim, J.I., and Huq, E. (2017). Expanding Roles of PIFs in Signal Integration from Multiple Processes. Mol. Plant *10*, 1035–1046. https://doi.org/10.1016/j.molp.2017.07.002.
6. Krahmer, J., and Fankhauser, C. (2024). Environmental Control of Hypocotyl Elongation. Annu. Rev. Plant Biol. *75*, 489–519. https://doi.org/10.1146/ANNUREV-ARPLANT-062923-023852.
7. Wang, Z.Y., and Tobin, E.M. (1998). Constitutive expression of the CIRCADIAN CLOCK ASSOCIATED 1 (CCA1) gene disrupts circadian rhythms and suppresses its own expression. Cell *93*, 1207–1217. https://doi.org/10.1016/S0092-8674(00)81464-6.
8. Xue, X., Sun, K., and Zhu, Z. (2020). CIRCADIAN CLOCK ASSOCIATED 1 gates morning phased auxin response in Arabidopsis thaliana. Biochem.

Biophys. Res. Commun. *527*, 935–940. https://doi.org/10.1016/J.BBRC.2020.05.049.

9. Wang, S., Sun, Q., Zhang, M., Yin, C., and Ni, M. (2021). WRKY2 and WRKY10 regulate the circadian expression of PIF4 during the day through interactions with CCA1/LHY and phyB. Plant Commun. *3*, 100265. https://doi.org/10.1016/J.XPLC.2021.100265.
10. Sun, Q., Wang, S., Xu, G., Kang, X., Zhang, M., and Ni, M. (2019). SHB1 and CCA1 interaction desensitizes light responses and enhances thermomorphogenesis. Nat. Commun. *10*, 3110. https://doi.org/10.1038/S41467-019-11071-6.
11. Ruts, T., Matsubara, S., Wiese-Klinkenberg, A., and Walter, A. (2012). Aberrant temporal growth pattern and morphology of root and shoot caused by a defective circadian clock in Arabidopsis thaliana. Plant J. *72*, 154–161. https://doi.org/10.1111/J.1365-313X.2012.05073.X.
12. Voß, U., Wilson, M.H., Kenobi, K., Gould, P.D., Robertson, F.C., Peer, W.A., Lucas, M., Swarup, K., Casimiro, I., Holman, T.J., et al. (2015). The circadian clock rephases during lateral root organ initiation in Arabidopsis thaliana. Nat. Commun. *6*, 7641. https://doi.org/10.1038/ncomms8641.
13. Ikeda, H., Uchikawa, T., Kondo, Y., Takahashi, N., Shishikui, T., Watahiki, M.K., Kubota, A., and Endo, M. (2023). Circadian Clock Controls Root Hair Elongation through Long-Distance Communication. Plant Cell Physiol. *64*, 1289–1300. https://doi.org/10.1093/pcp/pcad076.
14. Uemoto, K., Mori, F., Yamauchi, S., Kubota, A., Takahashi, N., Egashira, H., Kunimoto, Y., Araki, T., Takemiya, A., Ito, H., et al. (2023). Root PRR7 Improves the Accuracy of the Shoot Circadian Clock through Nutrient Transport. Plant Cell Physiol. *64*, 352–362. https://doi.org/10.1093/PCP/PCAD003.
15. Rayle, D.L., and Cleland, R. (1970). Enhancement of Wall Loosening and Elongation by Acid Solutions. Plant Physiol. *46*, 250–253. https://doi.org/10.1104/pp.46.2.250.
16. Cleland, R., and Haughton, P.M. (1971). The Effect of Auxin on Stress Relaxation in Isolated *Avena* Coleoptiles. Plant Physiol. *47*, 812–815. https://doi.org/10.1104/pp.47.6.812.
17. Hager, A., Menzel, H., and Krauss, A. (1971). Versuche und Hypothese zur Primärwirkung des Auxins Beim Streckungswachstum. Planta *100*, 47–75. https://doi.org/10.1007/BF00386886.
18. Li, L., Verstraeten, I., Roosjen, M., Takahashi, K., Rodriguez, L., Merrin, J., Chen, J., Shabala, L., Smet, W., Ren, H., et al. (2021). Cell surface and intracellular auxin signalling for H+ fluxes in root growth. Nature *599*, 273–277. https://doi.org/10.1038/s41586-021-04037-6.
19. Lin, W., Zhou, X., Tang, W., Takahashi, K., Pan, X., Dai, J., Ren, H., Zhu, X., Pan, S., Zheng, H., et al. (2021). TMK-based cell-surface auxin signalling activates cell-wall acidification. Nature *599*, 278–282. https://doi.org/10.1038/s41586-021-03976-4.
20. Friml, J., Gallei, M., Gelová, Z., Johnson, A., Mazur, E., Monzer, A., Rodriguez, L., Roosjen, M., Verstraeten, I., Živanović, B.D., et al. (2022). ABP1–TMK auxin perception for global phosphorylation and auxin canalization. Nature *609*, 575–581. https://doi.org/10.1038/s41586-022-05187-x.
21. Wang, J., Jin, D., Deng, Z., Zheng, L., Guo, P., Ji, Y., Song, Z., Zeng, H.Y., Kinoshita, T., Liao, Z., et al. (2025). The apoplastic pH is a key determinant in the hypocotyl growth response to auxin dosage and light. Nat. Plants *11*, 279–294. https://doi.org/10.1038/S41477-025-01910-4.
22. Falhof, J., Pedersen, J.T., Fuglsang, A.T., and Palmgren, M. (2016). Plasma Membrane H + -ATPase Regulation in the Center of Plant Physiology. Mol. Plant *9*, 323–337. https://doi.org/10.1016/j.molp.2015.11.002.
23. Michalak, A., Wdowikowska, A., and Janicka, M. (2022). Plant Plasma Membrane Proton Pump: One Protein with Multiple Functions. Cells *11*, 4052. https://doi.org/10.3390/cells11244052.
24. Haruta, M., Burch, H.L., Nelson, R.B., Barrett-Wilt, G., Kline, K.G., Mohsin, S.B., Young, J.C., Otegui, M.S., and Sussman, M.R. (2010). Molecular characterization of mutant Arabidopsis plants with reduced plasma membrane proton pump activity. J. Biol. Chem. *285*, 17918–17929. https://doi.org/10.1074/JBC.M110.101733.
25. Palmgren, M.G. (2001). PLANT PLASMA MEMBRANE H+-ATPases: Powerhouses for Nutrient Uptake. Annu. Rev. Plant Physiol. Plant Mol. Biol. *52*, 817–845. https://doi.org/10.1146/ANNUREV.ARPLANT.52.1.817.
26. Guo, A.-Y., Wu, W.-Q., Liu, W.-C., Zheng, Y., Bai, D., Li, Y., Xie, J., Guo, S., and Song, C.-P. (2024). C2-domain abscisic acid-related proteins regulate the dynamics of a plasma membrane H+-ATPase in response to alkali stress. Plant Physiol. *196*, 2784–2794. https://doi.org/10.1093/plphys/kiae464.
27. Yang, T.-H., Ch Formula See Text Telat, A., Kurenda, A., and Farmer, E.E. (2023). Mechanosensation in leaf veins. Sci. Adv. *9*, eadh5078. https://doi.org/10.1126/sciadv.adh5078.
28. Torne-Srivastava, T., Grunwald, Y., Dalal, A., Yaaran, A., Moshelion, M., and Moran, N. (2024). A tale of two pumps: Blue light and abscisic acid alter Arabidopsis leaf hydraulics via bundle sheath cell H+-ATPases. Plant Physiol. *195*, 2635–2651. https://doi.org/10.1093/plphys/kiae226.
29. Huang, S., Shen, Z., An, R., Jia, Q., Wang, D., Wei, S., Mu, J., and Zhang, Y. (2024). Identification and characterization of the plasma membrane H+-ATPase genes in Brassica napus and functional analysis of BnHA9 in salt tolerance. Plant Physiol. Biochem. *210*, 108566. https://doi.org/10.1016/j.plaphy.2024.108566.
30. Yuan, W., Zhang, D., Song, T., Xu, F., Lin, S., Xu, W., Li, Q., Zhu, Y., Liang, J., and Zhang, J. (2017). Arabidopsis plasma membrane H+-ATPase genes AHA2 and AHA7 have distinct and overlapping roles in the modulation of root tip H+ efflux in response to low-phosphorus stress. J. Exp. Bot. *68*, 1731–1741. https://doi.org/10.1093/JXB/ERX040.
31. Jiang, H., Su, J., Ren, Z., Wang, D., Hills, A., Kinoshita, T., Blatt, M.R., Wang, Y., and Wang, Y. (2024). Dual function of overexpressing plasma membrane H+-ATPase in balancing carbon-water use. Sci. Adv. *10*, eadp8017. https://doi.org/10.1126/sciadv.adp8017.
32. Robertson, W.R., Clark, K., Young, J.C., and Sussman, M.R. (2004). An Arabidopsis thaliana Plasma Membrane Proton Pump Is Essential for Pollen Development. Genetics *168*, 1677–1687. https://doi.org/10.1534/genetics.104.032326.
33. DeWitt, N.D., Harper, J.F., and Sussman, M.R. (1991). Evidence for a plasma membrane proton pump in phloem cells of higher plants. Plant J. *1*, 121–128. https://doi.org/10.1111/j.1365-313X.1991.00121.x.
34. DeWitt, N.D., and Sussman, M.R. (1995). Immunocytological localization of an epitope-tagged plasma membrane proton pump (H(+)-ATPase) in phloem companion cells. Plant Cell *7*, 2053–2067. https://doi.org/10.1105/tpc.7.12.2053.
35. Hoffmann, R.D., Portes, M.T., Olsen, L.I., Damineli, D.S.C., Hayashi, M., Nunes, C.O., Pedersen, J.T., Lima, P.T., Campos, C., Feijó, J.A., et al. (2020). Plasma membrane H+-ATPases sustain pollen tube growth and fertilization. Nat. Commun. *11*, 2395. https://doi.org/10.1038/S41467-020-16253-1.
36. Young, J.C., DeWitt, N.D., and Sussman, M.R. (1998). A transgene encoding a plasma membrane H+-ATPase that confers acid resistance in Arabidopsis thaliana seedlings. Genetics *149*, 501–507. https://doi.org/10.1093/GENETICS/149.2.501.
37. Zhao, R., Dielen, V., Kinet, J.M., and Boutry, M. (2000). Cosuppression of a plasma membrane H(+)-ATPase isoform impairs sucrose translocation, stomatal opening, plant growth, and male fertility. Plant Cell *12*, 535–546. https://doi.org/10.1105/TPC.12.4.535.
38. Braun, D.M. (2022). Phloem Loading and Unloading of Sucrose: What a Long, Strange Trip from Source to Sink. Annu. Rev. Plant Biol. *73*, 553–584. https://doi.org/10.1146/annurev-arplant-070721-083240.
39. Rolland, F., Baena-Gonzalez, E., and Sheen, J. (2006). Sugar sensing and signaling in plants: conserved and novel mechanisms. Annu. Rev. Plant

Biol. *57*, 675–709. https://doi.org/10.1146/ANNUREV.ARPLANT.57.032905.105441.

40. Sauer, N. (2007). Molecular physiology of higher plant sucrose transporters. FEBS Lett. *581*, 2309–2317. https://doi.org/10.1016/j.febslet.2007.03.048.
41. Gottwald, J.R., Krysan, P.J., Young, J.C., Evert, R.F., and Sussman, M.R. (2000). Genetic evidence for the *in planta* role of phloem-specific plasma membrane sucrose transporters. Proc. Natl. Acad. Sci. USA *97*, 13979–13984. https://doi.org/10.1073/pnas.250473797.
42. Kircher, S., and Schopfer, P. (2012). Photosynthetic sucrose acts as cotyledon-derived long-distance signal to control root growth during early seedling development in *Arabidopsis*. Proc. Natl. Acad. Sci. USA *109*, 11217–11221. https://doi.org/10.1073/pnas.1203746109.
43. Lemoine, R., La Camera, S., Atanassova, R., Dédaldéchamp, F., Allario, T., Pourtau, N., Bonnemain, J.L., Laloi, M., Coutos-Thévenot, P., Maurousset, L., et al. (2013). Source-to-sink transport of sugar and regulation by environmental factors. Front. Plant Sci. *4*, 272. https://doi.org/10.3389/FPLS.2013.00272.
44. Omelyanchuk, N.A., Wiebe, D.S., Novikova, D.D., Levitsky, V.G., Klimova, N., Gorelova, V., Weinholdt, C., Vasiliev, G.V., Zemlyanskaya, E.V., Kolchanov, N.A., et al. (2017). Auxin regulates functional gene groups in a fold-change-specific manner in Arabidopsis thaliana roots. Sci. Rep. *7*, 2489. https://doi.org/10.1038/S41598-017-02476-8.
45. Lee, S., Wang, W., and Huq, E. (2021). Spatial regulation of thermomorphogenesis by HY5 and PIF4 in Arabidopsis. Nat. Commun. *12*, 3656. https://doi.org/10.1038/S41467-021-24018-7.
46. Chen, L.Q., Qu, X.Q., Hou, B.H., Sosso, D., Osorio, S., Fernie, A.R., and Frommer, W.B. (2012). Sucrose efflux mediated by SWEET proteins as a key step for phloem transport. Science *335*, 207–211. https://doi.org/10.1126/SCIENCE.1213351.
47. Dasgupta, K., Khadilkar, A.S., Sulpice, R., Pant, B., Scheible, W.R., Fisahn, J., Stitt, M., and Ayre, B.G. (2014). Expression of Sucrose Transporter cDNAs Specifically in Companion Cells Enhances Phloem Loading and Long-Distance Transport of Sucrose but Leads to an Inhibition of Growth and the Perception of a Phosphate Limitation. Plant Physiol. *165*, 715–731. https://doi.org/10.1104/PP.114.238410.
48. Wang, X., Jiang, B., Gu, L., Chen, Y., Mora, M., Zhu, M., Noory, E., Wang, Q., and Lin, C. (2021). A photoregulatory mechanism of the circadian clock in Arabidopsis. Nat. Plants *7*, 1397–1408. https://doi.org/10.1038/S41477-021-01002-Z.
49. Xu, Q., and Liesche, J. (2021). Sugar export from Arabidopsis leaves: actors and regulatory strategies. J. Exp. Bot. *72*, 5275–5284. https://doi.org/10.1093/jxb/erab241.
50. Ryu, K.H., Huang, L., Kang, H.M., and Schiefelbein, J. (2019). Single-Cell RNA Sequencing Resolves Molecular Relationships Among Individual Plant Cells. Plant Physiol. *179*, 1444–1456. https://doi.org/10.1104/PP.18.01482.
51. Knox, K. (2019). Measuring Phloem Transport Velocity in Arabidopsis Seedlings Using the Fluorescent Coumarin Glucoside, Esculin. Methods Mol. Biol. *2014*, 195–201. https://doi.org/10.1007/978-1-4939-9562-2_16.
52. Moreau, H., Gaillard, I., and Paris, N. (2022). Genetically encoded fluorescent sensors adapted to acidic pH highlight subdomains within the plant cell apoplast. J. Exp. Bot. *73*, 6744–6757. https://doi.org/10.1093/JXB/ERAC210.
53. Matsuda, Y., Liang, G., Zhu, Y., Ma, F., Nelson, R.S., and Ding, B. (2002). The Commelina yellow mottle virus promoter drives companion-cell-specific gene expression in multiple organs of transgenic tobacco. Protoplasma *220*, 51–58. https://doi.org/10.1007/S00709-002-0027-6.
54. Medberry, S.L., Lockhart, B.E.L., and Olszewski, N.E. (1992). The Commelina yellow mottle virus promoter is a strong promoter in vascular and reproductive tissues. Plant Cell *4*, 185–192. https://doi.org/10.1105/TPC.4.2.185.
55. Ohara, T., and Satake, A. (2017). Photosynthetic entrainment of the circadian clock facilitates plant growth under environmental fluctuations: Perspectives from an integrated model of phase oscillator and phloem transportation. Front. Plant Sci. *8*, 307385. https://doi.org/10.3389/FPLS.2017.01859/BIBTEX.
56. Kircher, S., and Schopfer, P. (2023). Photosynthetic sucrose drives the lateral root clock in Arabidopsis seedlings. Curr. Biol. *33*, 2201–2212.e3. https://doi.org/10.1016/J.CUB.2023.04.061.
57. Mortada, M., Xiong, L., and Mas, P. (2024). Dissecting the complexity of local and systemic circadian communication in plants. npj Biol. Timing Sleep *1*, 1–7. https://doi.org/10.1038/s44323-024-00003-3.
58. Takahashi, N., Hirata, Y., Aihara, K., and Mas, P. (2015). A Hierarchical Multi-oscillator Network Orchestrates the Arabidopsis Circadian System. Cell *163*, 148–159. https://doi.org/10.1016/j.cell.2015.08.062.
59. James, A.B., Monreal, J.A., Nimmo, G.A., Kelly, C.L., Herzyk, P., Jenkins, G.I., and Nimmo, H.G. (2008). The circadian clock in Arabidopsis roots is a simplified slave version of the clock in shoots. Science *322*, 1832–1835. https://doi.org/10.1126/science.1161403.
60. Chen, W.W., Takahashi, N., Hirata, Y., Ronald, J., Porco, S., Davis, S.J., Nusinow, D.A., Kay, S.A., and Mas, P. (2020). A mobile ELF4 delivers circadian temperature information from shoots to roots. Nat. Plants *6*, 416–426. https://doi.org/10.1038/s41477-020-0634-2.
61. Mizoguchi, T., Wheatley, K., Hanzawa, Y., Wright, L., Mizoguchi, M., Song, H.R., Carré, I.A., and Coupland, G. (2002). LHY and CCA1 are partially redundant genes required to maintain circadian rhythms in Arabidopsis. Dev. Cell *2*, 629–641. https://doi.org/10.1016/S1534-5807(02)00170-3.
62. Alabadí, D., Yanovsky, M.J.J., Más, P., Harmer, S.L.L., Kay, S.A.A., Alabadi, D., Yanovsky, M.J.J., Mas, P., Harmer, S.L.L., and Kay, S.A.A. (2002). Critical role for CCA1 and LHY in maintaining circadian rhythmicity in Arabidopsis. Curr. Biol. *12*, 757–761. https://doi.org/10.1016/S0960-9822(02)00815-1.
63. Lu, S.X., Webb, C.J., Knowles, S.M., Kim, S.H.J., Wang, Z., and Tobin, E.M. (2012). CCA1 and ELF3 Interact in the Control of Hypocotyl Length and Flowering Time in Arabidopsis. Plant Physiol. *158*, 1079–1088. https://doi.org/10.1104/pp.111.189670.
64. Hughes, C.L., and Harmer, S.L. (2023). Myb-like transcription factors have epistatic effects on circadian clock function but additive effects on plant growth. Plant Direct *7*, e533. https://doi.org/10.1002/PLD3.533.
65. Gray, J.A., Shalit-Kaneh, A., Chu, D.N., Hsu, P.Y., and Harmer, S.L. (2017). The REVEILLE Clock Genes Inhibit Growth of Juvenile and Adult Plants by Control of Cell Size. Plant Physiol. *173*, 2308–2322. https://doi.org/10.1104/PP.17.00109.
66. Barbez, E., Dünser, K., Gaidora, A., Lendl, T., and Busch, W. (2017). Auxin steers root cell expansion via apoplastic pH regulation in Arabidopsis thaliana. Proc. Natl. Acad. Sci. USA. *114*, E4884–E4893. https://doi.org/10.1073/PNAS.1613499114.
67. Frank, A., Matiolli, C.C., Viana, A.J.C., Hearn, T.J., Kusakina, J., Belbin, F.E., Wells Newman, D., Yochikawa, A., Cano-Ramirez, D.L., Chembath, A., et al. (2018). Circadian Entrainment in Arabidopsis by the Sugar-Responsive Transcription Factor bZIP63. Curr. Biol. *28*, 2597–2606.e6. https://doi.org/10.1016/j.cub.2018.05.092.
68. Love, J., Dodd, A.N., and Webb, A.A.R. (2004). Circadian and diurnal calcium oscillations encode photoperiodic information in Arabidopsis. Plant Cell *16*, 956–966. https://doi.org/10.1105/tpc.020214.
69. Stitt, M., Lunn, J., and Usadel, B. (2010). Arabidopsis and primary photosynthetic metabolism - more than the icing on the cake. Plant J. *61*, 1067–1091. https://doi.org/10.1111/J.1365-313X.2010.04142.X.
70. Haydon, M.J., Mielczarek, O., Robertson, F.C., Hubbard, K.E., and Webb, A.A.R. (2013). Photosynthetic entrainment of the Arabidopsis thaliana circadian clock. Nature *502*, 689–692. https://doi.org/10.1038/nature12603.

71. Bläsing, O.E., Gibon, Y., Günther, M., Höhne, M., Morcuende, R., Osuna, D., Thimm, O., Usadel, B.B., Scheible, W.-R.R., and Stitt, M. (2005). Sugars and circadian regulation make major contributions to the global regulation of diurnal gene expression in Arabidopsis. Plant Cell *17*, 3257–3281. https://doi.org/10.1105/tpc.105.035261.

72. Dalchau, N., Baek, S.J., Briggs, H.M., Robertson, F.C., Dodd, A.N., Gardner, M.J., Stancombe, M.A., Haydon, M.J., Stan, G.-B., Gonçalves, J.M., et al. (2011). The circadian oscillator gene GIGANTEA mediates a long-term response of the Arabidopsis thaliana circadian clock to sucrose. Proc. Natl. Acad. Sci. USA *108*, 5104–5109. https://doi.org/10.1073/pnas.1015452108.

73. Viana, A.J.C., Matiolli, C.C., Newman, D.W., Vieira, J.G.P., Duarte, G.T., Martins, M.C.M., Gilbault, E., Hotta, C.T., Caldana, C., and Vincentz, M. (2021). The sugar-responsive circadian clock regulator bZIP63 modulates plant growth. New Phytol. *231*, 1875–1889. https://doi.org/10.1111/NPH.17518.

74. Yazdanbakhsh, N., Sulpice, R., Graf, A., Stitt, M., and Fisahn, J. (2011). Circadian control of root elongation and C partitioning in Arabidopsis thaliana. Plant Cell Environ. *34*, 877–894. https://doi.org/10.1111/J.1365-3040.2011.02286.X.

75. De Wit, M., George, G.M., Ince, Y.Ç., Dankwa-Egli, B., Hersch, M., Zeeman, S.C., and Fankhauser, C. (2018). Changes in resource partitioning between and within organs support growth adjustment to neighbor proximity in Brassicaceae seedlings. Proc. Natl. Acad. Sci. USA *115*, E9953–E9961. https://doi.org/10.1073/pnas.1806084115.

76. Graf, A., Schlereth, A., Stitt, M., and Smith, A.M. (2010). Circadian control of carbohydrate availability for growth in Arabidopsis plants at night. Proc. Natl. Acad. Sci. USA *107*, 9458–9463. https://doi.org/10.1073/pnas.0914299107.

77. Alexandre Moraes, T.A., Mengin, V., Peixoto, B., Encke, B., Krohn, N., Höhne, M., Krause, U., and Stitt, M. (2022). The circadian clock mutant lhy cca1 elf3 paces starch mobilization to dawn despite severely disrupted circadian clock function. Plant Physiol. *189*, 2332–2356. https://doi.org/10.1093/PLPHYS/KIAC226.

78. Krahmer, J., Hindle, M., Perby, L.K., Mogensen, H.K., Nielsen, T.H., Halliday, K.J., van Ooijen, G., Le Bihan, T., and Millar, A.J. (2021). The Circadian Clock Gene Circuit Controls Protein and Phosphoprotein Rhythms in Arabidopsis thaliana. Mol. Cell. Proteomics *21*, 100172. https://doi.org/10.1016/J.MCPRO.2021.100172.

79. Yu, Q., Tang, C., and Kuo, J. (2000). A critical review on methods to measure apoplastic pH in plants. Plant Soil *219*, 29–40. https://doi.org/10.1023/A:1004724610550.

80. Hafke, J.B., Van Amerongen, J.K., Kelling, F., Furch, A.C.U., Gaupels, F., and Van Bel, A.J.E. (2005). Thermodynamic battle for photosynthate acquisition between sieve tubes and adjoining parenchyma in transport phloem. Plant Physiol. *138*, 1527–1537. https://doi.org/10.1104/PP.104.058511.

81. Ainsworth, E.A., and Bush, D.R. (2011). Carbohydrate export from the leaf: a highly regulated process and target to enhance photosynthesis and productivity. Plant Physiol. *155*, 64–69. https://doi.org/10.1104/PP.110.167684.

82. Braun, D.M., Wang, L., and Ruan, Y.L. (2014). Understanding and manipulating sucrose phloem loading, unloading, metabolism, and signalling to enhance crop yield and food security. J. Exp. Bot. *65*, 1713–1735. https://doi.org/10.1093/JXB/ERT416.

83. Yadav, U.P., Ayre, B.G., and Bush, D.R. (2015). Transgenic approaches to altering carbon and nitrogen partitioning in whole plants: assessing the potential to improve crop yields and nutritional quality. Front. Plant Sci. *6*, 275. https://doi.org/10.3389/FPLS.2015.00275.

84. Majumdar, R., Barchi, B., Turlapati, S.A., Gagne, M., Minocha, R., Long, S., and Minocha, S.C. (2016). Glutamate, Ornithine, Arginine, Proline, and Polyamine Metabolic Interactions: The Pathway Is Regulated at the Post-Transcriptional Level. Front. Plant Sci. *7*, 78. https://doi.org/10.3389/fpls.2016.00078.

85. Okumura, M., Inoue, S.I., Kuwata, K., and Kinoshita, T. (2016). Photosynthesis activates plasma membrane H+-ATPase via sugar accumulation. Plant Physiol. *171*, 580–589. https://doi.org/10.1104/PP.16.00355.

86. Sussman, M.R., and Harper, J.F. (1989). Molecular biology of the plasma membrane of higher plants. Plant Cell *1*, 953–960. https://doi.org/10.1105/TPC.1.10.953.

87. Zhang, L.Y., Peng, Y.B., Pelleschi-Travier, S., Fan, Y., Lu, Y.F., Lu, Y.M., Gao, X.P., Shen, Y.Y., Delrot, S., and Zhang, D.P. (2004). Evidence for Apoplasmic Phloem Unloading in Developing Apple Fruit. Plant Physiol. *135*, 574–586. https://doi.org/10.1104/PP.103.036632.

88. Khadilkar, A.S., Yadav, U.P., Salazar, C., Shulaev, V., Paez-Valencia, J., Pizzio, G.A., Gaxiola, R.A., and Ayre, B.G. (2015). Constitutive and Companion Cell-Specific Overexpression of AVP1, Encoding a Proton-Pumping Pyrophosphatase, Enhances Biomass Accumulation, Phloem Loading, and Long-Distance Transport. Plant Physiol. *170*, 401–414. https://doi.org/10.1104/PP.15.01409.

89. Carpaneto, A., Geiger, D., Bamberg, E., Sauer, N., Fromm, J., and Hedrich, R. (2005). Phloem-localized, proton-coupled sucrose carrier ZmSUT1 mediates sucrose efflux under the control of the sucrose gradient and the proton motive force. J. Biol. Chem. *280*, 21437–21443. https://doi.org/10.1074/jbc.M501785200.

90. Nitschke, S., Cortleven, A., Iven, T., Feussner, I., Havaux, M., Riefler, M., and Schmülling, T. (2016). Circadian Stress Regimes Affect the Circadian Clock and Cause Jasmonic Acid-Dependent Cell Death in Cytokinin-Deficient Arabidopsis Plants. Plant Cell *28*, 1616–1639. https://doi.org/10.1105/TPC.16.00016.

91. Hicks, K.A., Millar, A.J., Carré, I.A., Somers, D.E., Straume, M., Meeks-Wagner, D.R., and Kay, S.A. (1996). Conditional circadian dysfunction of the Arabidopsis early-flowering 3 mutant. Science *274*, 790–792. https://doi.org/10.1126/science.274.5288.790.

92. Huang, H., Alvarez, S., Bindbeutel, R., Shen, Z., Naldrett, M.J., Evans, B.S., Briggs, S.P., Hicks, L.M., Kay, S.A., and Nusinow, D.A. (2016). Identification of Evening Complex Associated Proteins in Arabidopsis by Affinity Purification and Mass Spectrometry. Mol. Cell Proteomics. *15*, 201–217. https://doi.org/10.1074/mcp.M115.054064.

93. Nakamichi, N., Kita, M., Ito, S., Yamashino, T., and Mizuno, T. (2005). PSEUDO-RESPONSE REGULATORS, PRR9, PRR7 and PRR5, together play essential roles close to the circadian clock of Arabidopsis thaliana. Plant Cell Physiol. *46*, 686–698. https://doi.org/10.1093/pcp/pci086.

94. Farré, E.M., Harmer, S.L., Harmon, F.G., Yanovsky, M.J., and Kay, S.A. (2005). Overlapping and distinct roles of PRR7 and PRR9 in the Arabidopsis circadian clock. Curr. Biol. *15*, 47–54. https://doi.org/10.1016/j.cub.2004.12.067.

95. Yakir, E., Hilman, D., Kron, I., Hassidim, M., Melamed-Book, N., and Green, R.M. (2009). Posttranslational Regulation of CIRCADIAN CLOCK ASSOCIATED1 in the Circadian Oscillator of Arabidopsis. Plant Physiol. *150*, 844–857. https://doi.org/10.1104/pp.109.137414.

96. Carrington, J.C., Freed, D.D., and Leinicke, A.J. (1991). Bipartite signal sequence mediates nuclear translocation of the plant potyviral NIa protein. Plant Cell *3*, 953–962. https://doi.org/10.1105/tpc.3.9.953.

97. Hajdukiewicz, P., Svab, Z., and Maliga, P. (1994). The small, versatile pPZP family of Agrobacterium binary vectors for plant transformation. Plant Mol. Biol. *25*, 989–994. https://doi.org/10.1007/BF00014672.

98. Michael, T.P., Mockler, T.C., Breton, G., McEntee, C., Byer, A., Trout, J.D., Hazen, S.P., Shen, R., Priest, H.D., Sullivan, C.M., et al. (2008). Network discovery pipeline elucidates conserved time-of-day-specific cis-regulatory modules. PLoS Genet. *4*, e14. https://doi.org/10.1371/journal.pgen.0040014.

99. Mockler, T.C., Michael, T.P., Priest, H.D., Shen, R., Sullivan, C.M., Givan, S.A., McEntee, C., Kay, S.A., and Chory, J. (2007). The DIURNAL project: DIURNAL and circadian expression profiling, model-based pattern matching, and promoter analysis. Cold Spring Harb. Symp. Quant. Biol. *72*, 353–363. https://doi.org/10.1101/sqb.2007.72.006.

100. Clough, S.J., and Bent, A.F. (1998). Floral dip: A simplified method for Agrobacterium-mediated transformation of Arabidopsis thaliana. Plant J. *16*, 735–743. https://doi.org/10.1046/j.1365-313X.1998.00343.x.

101. Silva-Navas, J., Moreno-Risueno, M.A., Manzano, C., Pallero-Baena, M., Navarro-Neila, S., Téllez-Robledo, B., Garcia-Mina, J.M., Baigorri, R., Gallego, F.J., and Del Pozo, J.C. (2015). D-Root: a system for cultivating plants with the roots in darkness or under different light conditions. Plant J. *84*, 244–255. https://doi.org/10.1111/TPJ.12998.

102. Kim, D., Paggi, J.M., Park, C., Bennett, C., and Salzberg, S.L. (2019). Graph-based genome alignment and genotyping with HISAT2 and HISAT-genotype. Nat. Biotechnol. *37*, 907–915. https://doi.org/10.1038/s41587-019-0201-4.

103. Liao, Y., Smyth, G.K., and Shi, W. (2014). featureCounts: an efficient general purpose program for assigning sequence reads to genomic features. Bioinformatics *30*, 923–930. https://doi.org/10.1093/bioinformatics/btt656.

104. Babicki, S., Arndt, D., Marcu, A., Liang, Y., Grant, J.R., Maciejewski, A., and Wishart, D.S. (2016). Heatmapper: web-enabled heat mapping for all. Nucleic Acids Res. *44*, W147–W153. https://doi.org/10.1093/nar/gkw419.

105. Czechowski, T., Stitt, M., Altmann, T., Udvardi, M.K., and Scheible, W.-R. (2005). Genome-Wide Identification and Testing of Superior Reference Genes for Transcript Normalization in Arabidopsis. Plant Physiol. *139*, 5–17. https://doi.org/10.1104/pp.105.063743.

106. Yamaguchi, N., Winter, C.M., Wu, M.-F., Kwon, C.S., William, D.A., and Wagner, D. (2014). PROTOCOLS: Chromatin Immunoprecipitation from Arabidopsis Tissues. Arabidopsis Book *12*, e0170. https://doi.org/10.1199/tab.0170.

107. Kaplan, F., and Guy, C.L. (2005). RNA interference of Arabidopsis beta-amylase8 prevents maltose accumulation upon cold shock and increases sensitivity of PSII photochemical efficiency to freezing stress. Plant J. *44*, 730–743. https://doi.org/10.1111/J.1365-313X.2005.02565.X.

Please cite this article in press as: Xiong et al., A circadian rheostat drives proton electrochemical gradients to optimize cell-type-specific growth in *Arabidopsis*, Cell (2026), https://doi.org/10.1016/j.cell.2025.12.056

STAR★METHODS

KEY RESOURCES TABLE

REAGENT or RESOURCE	SOURCE	IDENTIFIER
Antibodies		
GFP Polyclonal Antibody	Thermo Fisher Scientific (Invitrogen)	Cat#A-11122; RRID: AB_221569
CCA1 (C) Antibody, Rabbit Polyclonal	Abiocode	Cat#R1234-3
Bacterial and virus strains		
Agrobacterium tumefaciens (strain GV3101)	N/A	N/A
Chemicals, peptides, and recombinant proteins		
Dynabeads™ Protein G for Immunoprecipitation	Thermo Fisher Scientific (Invitrogen)	Cat#10004D
Esculin sesquihydrate, 97%	Thermo Fisher Scientific	Cat#A11624-06
8-Hydroxy-1,3,6-pyrenetrisulfonic acid trisodium salt (HPTS), 98%	Thermo Fisher Scientific	Cat#412180010
Critical commercial assays		
RNeasy Plant Mini Kit for RNA Extraction	QIAGEN	Cat#74904
RNase-Free DNase Set	QIAGEN	Cat#79254
Maxwell® RSC Plant RNA Kit	Promega	Cat#AS1500
PrimeScript™ RT Master Mix (Perfect Real Time)	Takara Bio	Cat#RR036B
TB Green® Premix Ex Taq™ II (Tli RNaseH Plus)	Takara Bio	Cat#RR820W
Deposited data		
Source code	This study	GitHub: https://github.com/seki-design/sucrose-transport
RNA-Seq data	This study	Mendeley Data: http://www.doi.org/10.17632/3jgj3b365r.1 and GEO: GSE315134
Experimental models: Organisms/strains		
Arabidopsis thaliana: WT Columbia (Col-0)	Nottingham Arabidopsis Stock Centre (NASC)	N6673
Arabidopsis thaliana: CCA1-ox	Wang et al.[7]	N/A
Arabidopsis thaliana: *cca1-1/lhy-20*	Nitschke et al.[90]	N/A
Arabidopsis thaliana: *elf3-2*	Hicks et al.[91]	N/A
Arabidopsis thaliana: *elf4-2*	Huang et al.[92]	N/A
Arabidopsis thaliana: *prr579*	Nakamichi et al.[93]	N/A
Arabidopsis thaliana: *prr79*	Farré et al.[94]	N/A
Arabidopsis thaliana: *prr7*	Farré et al.[94]	N/A
Arabidopsis thaliana: *CCA1::CCA1-HA-YFP/cca1-1*	Yakir et al.[95]	N/A
Arabidopsis thaliana: *CoYMV::CCA1-HA-YFP/cca1-1*	This study	N/A
Arabidopsis thaliana: *PM-Apo-Acidin4*/Columbia	Moreau et al.[52]	N/A
Arabidopsis thaliana: *PM-Apo-Acidin4*/CCA1-ox	This study	N/A
Arabidopsis thaliana: *CoYMV::PM-Apo-Acidin4*/Columbia	This study	N/A
Arabidopsis thaliana: *CoYMV::PM-Apo-Acidin4*/CCA1-ox	This study	N/A
Oligonucleotides		
Primers used in this study	This study	Document S1; Table S2

(*Continued on next page*)

Continued

REAGENT or RESOURCE	SOURCE	IDENTIFIER
Recombinant DNA		
pRTL2 vector	Carrington et al.[96]	N/A
pPZP200 vector	Hajdukiewicz et al.[97]	N/A
pDONR207 vector	Thermo Fisher Scientific (Invitrogen)	N/A
pGPTV-*CoYMV::CmR-ccdB* vector	Dasgupta et al.[47]	N/A
35S::PM-Apo-Acidin4 vector	Moreau et al.[52]	N/A
pRTL2-*35::SUC2-MYC*	This study	N/A
pPZP200-*35::SUC2-MYC*	This study	N/A
pRTL2-*35::AHA3*	This study	N/A
pPZP200-*35::AHA3*	This study	N/A
pDONR207-*CCA1-YFP-HA*	This study	N/A
pGPTV-*CoYMV::CCA1-YFP-HA*	This study	N/A
pDONR207-*PM-Apo-Acidin4*	This study	N/A
pGPTV-*CoYMV:: PM-Apo-Acidin4*	This study	N/A
Software and algorithms		
DIURNAL database	Michael et al.[98]; Mockler et al.[99]	http://diurnal.mocklerlab.org/
GraphPad Prism	GraphPad Software	https://www.graphpad.com/scientific-software/prism/
Fiji (ImageJ) Life-Line version (2015 December 22)	Fiji (ImageJ)	https://imagej.net/software/fiji/downloads
FIJI-MACRO FOR RATIOMETRIC IMAGE CONVERSION	Barbez et al.[66]	N/A

EXPERIMENTAL MODEL AND STUDY PARTICIPANT DETAILS

Plant material and growing conditions

Arabidopsis thaliana Columbia (Col-0) plants were used as Wild-Type. The CCA1-ox,[7] *cca1-1/lhy-20*[90] (with the *cca1-1* backcrossed six times into the Col-0 background),[95] *elf3-2*,[91] *prr579*,[93] *prr79*,[94] *prr7*[94] and CCA1-HA-YFP/*cca1-1*[95] lines were described elsewhere. Seeds were surface-sterilized using 15% bleach for 10 min followed by 3 washes with sterilized distilled H_2O. Seeds were then sown on Petri dishes containing Murashige and Skoog (MS) medium containing vitamins (Duchefa), without or with sucrose at the different concentrations specified in the main text. Seeds were stratified at 4°C in the dark for 4 days, and germination was induced with 6 hours of white light (80 μE) at 22 °C followed by 18 hours of darkness.

The 35::*SUC2-MYC* over-expressing vector was generated by PCR-mediated amplification of the coding region (CDS) of the *SUC2* gene (AT1G22710) followed by four copies of the MYC epitope tag. The 35::*AHA3* was generated by PCR-mediated amplification of the CDS of the *AHA3* gene (AT5G57350). The amplified sequences were cloned downstream of the CaMV 35S promoter in the pRTL2 vector.[96] The plasmids were sub-cloned into the plant expression vector pPZP200.[97] The double SUC2-ox/CCA1-ox and AHA3-ox/CCA1-ox plants were generated by *Agrobacterium*-mediated plant transformation with the 35::*SUC2-MYC* construct or the 35::*AHA3* construct into CCA1-ox plants. The *CoYMV::CCA1-HA-YFP* vector (expressing *CCA1* specifically in companion cells) was generated by sub-cloning the *CCA1-HA-YFP* sequence from the *CCA1prom::CCA1-HA-YFP* vector[95] into the pDONR207 vector (Invitrogen). The *CCA1-HA-YFP* was subsequently sub-cloned into the plant expression vector pGPTV-*CoYMVp::CmR-ccdB*.[47] The CCA1-ox plants expressing the PM-Apo-Acidin4 were generated by crossing the PM-Apo-Acidin4 line[52] (kindly provided by Prof. N. Paris, IPSiM, Univ Montpellier, CNRS, INRAE, Montpellier, France) with the CCA1-ox plants. The *CoYMV::PM-Apo-Acidin4* vector (expressing *PM-Apo-Acidin4* specifically in companion cells) was generated by sub-cloning the *PM-Apo-Acidin4* sequence from the *35S::PM-Apo-Acidin4* vector[52] into the *pDONR207* vector (Invitrogen). The *PM-Apo-Acidin4* was subsequently sub-cloned into the plant expression vector *pGPTV-CoYMVp::CmR-ccdB*.[47] All the expression vectors were transformed into *Agrobacterium tumefaciens* (GV3101) and *Arabidopsis thaliana* plants were transformed via the floral dip method.[100]

METHOD DETAILS

Hypocotyl and root length measurements

Seeds were sterilized and stratified as described above and grown in MS agar medium without or with different sucrose concentrations. Seedlings were grown under 12h light: 12h dark cycles or under constant light conditions without prior entrainment (cool white

Please cite this article in press as: Xiong et al., A circadian rheostat drives proton electrochemical gradients to optimize cell-type-specific growth in *Arabidopsis*, Cell (2026), https://doi.org/10.1016/j.cell.2025.12.056

fluorescent lights at the specified intensities) at 22°C for 8 days after germination. Plates were vertically oriented with an angle of approximately 70°. Measurements of roots kept in the dark (DR) while hypocotyls were illuminated was performed essentially as previously described.[101] Briefly, plates were covered with black aluminum foil and a black aluminum foil comb was fitted into the agar to separate the roots from the shoots and thereby excluding light exposure to the roots. Pictures were taken with a Nikon Z50 camera. Hypocotyl and root analyses were performed by measuring the length using the ImageJ software (https://imagej.net/ij/). For diel time course analyses, seeds were grown under 12h light: 12h dark cycles (white fluorescent light, 15 μE) at 22 °C. Images were taken every 4 hours with a stereomicroscope (Olympus, SZX16) from Zeitgeber Time 23 (ZT23) on the 6th Day to ZT23 on the 7th day. For developmental time course analyses, seeds were grown under constant white fluorescent light (15 μE) at 22 °C and images were taken with a stereomicroscope (Olympus, SZX16), starting from the day that cotyledons emerged from the seed coat.

RNA-seq analysis

Seedlings were grown under constant light conditions without prior entrainment (15 μE of white fluorescent light) at 22°C and samples were collected at 8 days after germination. Total RNA was isolated using a RNeasy Plant Mini Kit including on-column DNase digestion with the RNase-Free DNase Set (Qiagen). RNA purity was checked using a NanoPhotometer® spectrophotometer (IMPLEN, CA, USA), and RNA integrity and quantitation were assessed using the RNA Nano 6000 Assay Kit of the Bioanalyzer 2100 system (Agilent Technologies). Sequencing was performed by Novogene Co., Ltd. Sequencing libraries were generated using the Novogene NGS Stranded RNA Library Prep Set (PT044). mRNA was purified from total RNA using poly-T oligo-attached magnetic beads. The RNA was randomly fragmented using Bioruptor. These RNA fragments were subjected to reverse transcription and complementary strand synthesis, with the aim of obtaining double-stranded cDNA molecules. The double-stranded cDNA was end-polished with exonuclease/polymerase enzymes to create blunt ends, followed by adenylation of the 3′ ends, and ligated with the adapters. The fragments were analyzed by Agilent 5400 Fragment Analyzer. Libraries were amplified by PCR, and sequencing was performed using the Novaseq X Plus sequencing system (Illumina) with a paired-end read strategy of 150 bp per read (PE150).

Clustering of the index-coded samples was performed on a cBot Cluster Generation System using the PE Cluster Kit cBot-HS (Illumina) according to the manufacturer's instructions. After clustering, the library preparations were sequenced on an Illumina platform, and paired-end reads were generated. Raw data (raw reads) in FASTQ format were first processed using in-house Perl scripts. Clean reads were obtained by removing reads containing adapter and poly-N sequences and reads with low quality. Q20, Q30, and GC content of the clean data were calculated. All downstream analyses were based on the high-quality clean data. Paired-end clean reads were mapped to the reference genome using HISAT2 software v2.0.5.[102] FeatureCounts v1.5.0-p3[103] was used to count the read numbers mapped to each gene. FPKM (Fragments per kilobase of transcript sequence per Million base pairs sequenced) of each gene was calculated based on the length of the gene and the read count mapped to this gene.

The web-based tool "Heatmapper" was used to visualize data as heatmaps.[104] The circadian phases of expression were analyzed using the publicly available Gene Phase Analysis Tool "PHASER" of the DIURNAL database (http://diurnal.mocklerlab.org/).[98,99] Phase over-representation is calculated as the number of genes with a given phase divided by the total number of genes over the number of genes called rhythmic and divided by the total number of genes in the dataset. Circadian genes were classified into broad functional categories using the PANTHER Over-representation Test (Fisher's exact test, Bonferroni correction).

pH analyses

Ratiometric analyses of the pH sensor were essentially performed as previously described[52] using 8-day old seedlings and grown under constant light conditions without previous entrainment (at 15 μE of white fluorescent light). Analyses were also performed every 4 hours over a 24-h diel cycle (12h light: 12h darkness). For *CoYMV*::PM-Apo-Acidin4 pH sensor analyses, 3-day old seedlings were grown under constant light conditions without previous entrainment (at 15 μE of white fluorescent light). Signals from the pH sensor were imaged using the confocal microscope (Zeiss Elyra 7) with a ×40 water objective (LD LCI Plan-Apochromat 40x/1.2 Imm Corr DIC M27). mRFP was excited at 561 nm, and emitted light was recorded at 580–650 nm. SYFP2 was excited at 488 nm, and emitted light was recorded at 510–554 nm. Ratiometric images of the pH sensor and HPTS staining were obtained for each pixel by dividing the 488 nm intensity by the 561 nm intensity. Ratiometric image conversion was performed in Fiji (Life-Line version, 2015 December 22) using the macro language previously described.[66] Briefly, two-channel images (488 nm and 561 nm) were imported to Fiji, converted to 32-bit format, and subjected to Gaussian blurring for noise reduction. Channel 1 (488 nm) was used for segmentation by background subtraction and Laplacian of Gaussian filtering (FeatureJ plugin) to generate a binary mask. Ratiometric images were generated by pixel-wise division of channel 1 (488 nm) by channel 2 (561 nm) and multiplied by the segmentation mask to restrict analysis to cell wall regions. The display range was adjusted as appropriate. Final ratiometric images were exported as 32-bit TIFF files with calibration bars. HPTS staining was performed as previously described.[66] Four-day-old seedlings grown under constant light conditions (15 μE) without prior entrainment were incubated for 30 minutes in liquid MS medium containing 10 mM HPTS and imaged in the same HPTS-containing medium on a microscopy slide under a coverslip. Imaging was conducted using a confocal microscope (Zeiss Elyra 7) with a ×40 water objective (LD LCI Plan-Apochromat 40x/1.2 Imm Corr DIC M27). Protonated HPTS was excited at 405 nm and deprotonated HPTS at 488 nm, with emitted light collected at 500–580 nm for both forms. Ratiometric images were obtained by dividing the 488 nm intensity by the 405 nm intensity for each pixel, performed in Fiji (Life-Line version, 2015 December 22) using the macro language previously described.[66]

Phloem transport velocity

Phloem transport velocity analyses using the fluorescent sucrose analog were essentially performed as previously described.[51] For hypocotyl analyses, seedlings were grown under constant light conditions without previous entrainment (15 μE of white fluorescent light), and at 8 days after germination, each cotyledon was treated with 0.3 μl of 2.5% Adigor (Syngenta) for 5 minutes. Following Adigor careful removal with blotting paper, 0.3 μl of esculin (A11624-06, Thermo Fisher Scientific) was added to each cotyledon. For analyses of transport velocity in roots, seedlings grown under constant white fluorescent light (80 μE) at 22 °C for 4 days were subsequently transferred to constant white fluorescent light at 15 μE intensity for 3 days. The esculin position was recorded every minute after loading. Ten minutes after loading esculin, the first position of the visible esculin in the phloem was marked, and the time was recorded. After 5–10 minutes, seedlings were imaged again, marking the new front of esculin and recording the time. All images were taken by the stereomicroscope (Olympus, SZX16) equipped with a white LED illumination system (CoolLED pE-300^{lite}) and the UV Filter set (SZX2-FUV, Olympus, Ex:330–385). The distance between the two marks was calculated using ImageJ software (https://imagej.net/ij/), and the velocity was obtained by dividing the distance by the time.

Gene expression analysis by RT-qPCR

Shoots and roots (approximately 20 mg each) were collected from 8-day-old seedlings grown under constant light conditions (15 μE) without previous entrainment. Total RNA was isolated using the Maxwell RSC Plant RNA kit (Promega) following the manufacturer's recommendations. Single-strand cDNA was synthesized using the PrimeScript™ RT Master Mix (Perfect Real Time) for RT-qPCR (Takara Bio) following the manufacturer's recommendations. For qPCR analysis, cDNAs were diluted 10-fold with nuclease-free water, and qPCR was performed with TB Green™ Premix Ex Taq™ II (Tli RNaseH Plus) (Takara Bio) in a 96-well CFX96 Touch Real-Time PCR Detection System (Bio-Rad). The *PP2AA3* (AT1G13320)[105] was used as a control in both shoots and roots. The list of primers is included in Table S2.

Chromatin immunoprecipitation assays

ChIP assays were performed essentially as previously described.[106] For CCA1 minigene (CMG), seedlings were grown under diel cycles (12h light: 12h darkness) and samples were taken 8 days after gemination at Zeitgeber Time 3 (ZT3). For CCA1-ox, seedlings were grown under constant light conditions without prior entrainment and samples were taken 8 days after gemination. About 500 mg of shoots and 500 mg of roots were sampled, and vacuum infiltrated for 15 min in cross-linking solution (1% formaldehyde in 1×PBS) at room temperature. The cross-linking reaction was stopped by adding glycine to a final concentration of 0.125 M and vacuum infiltrated for 5 min. Samples were washed three times with cold deionized water, dried with paper towels and snapped-frozen in liquid nitrogen. Samples were ground to fine powder and extracted with 2.5 ml of Nuclei extraction buffer. After filtering the samples through Miracloth (475855, Merck), the chromatin solution was sonicated until obtaining sheared DNA of about 200–600 bp. Soluble chromatin was incubated overnight at 4°C with the anti-GFP antibody (A-11122, Thermo Fisher Scientific) or the anti-CCA1 antibody (R1234-3, Abiocode). Samples were then incubated with Protein G-Dynabeads beads (10004D, Thermo Fisher Scientific) for 4 hours at 4°C with rotation. The beads were washed thrice with Low salt wash buffer, High salt wash buffer, 250 mM LiCl wash buffer and 0.5×TE, respectively. The samples were eluted from the beads with 100 μL Nuclei Lysis buffer by incubating for 30 min at 65°C two times. The purified DNA was combined and QPCR was performed with TB Green™ Premix Ex Taq™ II (Tli RNaseH Plus) (Takara Bio) in a 96-well CFX96 Touch Real-Time PCR Detection System (BioRad). The list of primers is included in Table S2.

Analyses of sucrose content and starch accumulation

For analyses of sucrose content, sterilized seeds were planted on MS media (without sucrose) and stratified at 4 °C in darkness for 4 days. Seedlings were grown under constant white fluorescent light (100 μE) at 22 °C for 2 weeks and subsequently transferred to constant white fluorescent light (15 μE) at 22 °C for 3 days. Roots were collected and lyophilized overnight. For extraction, the lyophilized and homogenized roots (100 mg) were treated with 80% ethanol (10 mg/ml) and shaken at 80 °C overnight. The mixture was then centrifuged at 16,000 *g* for 15 minutes, and the supernatant was collected. The supernatant was mixed with water and chloroform in a 2:1:1 ratio and centrifuged at 16,000 *g* for 5 minutes. The upper aqueous phase was subjected to vacuum rotary evaporation at 60 °C until dry. To dissolve the residue, 0.1 ml of 80% acetonitrile (HPLC grade) was added, followed by centrifugation at 16,000 *g* for 5 minutes. The resulting solution (60 μL) was then analyzed using high-performance liquid chromatography (HPLC). HPLC analysis was conducted using an Agilent 1200 HPLC system with a refractive index detector (Agilent Technologies, Santa Clara, CA, USA) and equipped with an Agilent Zorbax carbohydrate Analysis Column. A 20 μL injection was made, using an 80% acetonitrile mobile phase at a flow rate of 1.0 mL/min, with both the detector and column maintained at 35 °C.

For starch analysis, 8-day-old seedlings grown under constant white fluorescent light (15 μE) were immersed in ethanol overnight to remove pigments and then stained with the iodine/potassium iodide solution (Lugol solution, 62650, Sigma) for 30 minutes. After two brief washes with water, the samples were preserved in water before taking pictures. The starch content was quantified using a colorimetric method as described previously[107]=with some modifications. Briefly, lyophilized and homogenized leaves (30 mg) were washed three times with ethanol to remove pigments. Following vacuum drying, the samples were solubilized in 1 mL water and shaken at 100 °C for 30 min. After cooling to room temperature, the solution was centrifuged and the supernatant was mixed with 10% Lugol's solution (62650, Sigma) at a 1:9 (v/v) ratio. The absorbance was measured at 620 nm. Potato starch (S2004, Sigma) was used as a standard for quantification.

Please cite this article in press as: Xiong et al., A circadian rheostat drives proton electrochemical gradients to optimize cell-type-specific growth in *Arabidopsis*, Cell (2026), https://doi.org/10.1016/j.cell.2025.12.056

Mathematical modelling

We simulated growth of root length (W) using a previously reported model,[55] with a slight modification: the model was simplified to include a single source (leaf) and a single sink (root), and root length was used as the output variable instead of root biomass. Sucrose translocation was simulated using parameter values provided in the original study. Since the conversion rate from sucrose (S) to growth, denoted as λ in Equation. (1) was not specified, we first estimated λ using time-series root growth data from WT plants.

$$\frac{d}{dt}W(t) = \lambda\alpha(S). \quad \text{(Equation 1)}$$

In the above equation, $\alpha(S)$represents the sucrose consumption rate for growth, which depends on the sucrose content S, as defined in the original study. Because the present model focuses on root length growth rather than biomass, we did not adopt the original assumption that growth rate is proportional to biomass.[55] In addition, because the light intensity used in our experiment differed from that of the previous study, we explored a range of values for the photosynthetic rate parameter (a) and performed model fitting for each setting. Because the experiment was conducted under constant light conditions, we simulated the model accordingly under constant light.

To evaluate how the sucrose loading rate to the phloem differs in CCA1-ox and *cca1lhy* mutant, we estimated the sucrose loading rate (η_G) in CCA1-ox and *cca1lhy* using time-series growth data, assuming that all other model parameters were identical to those estimated for WT. Only the sucrose loading rate parameter was allowed to vary between WT, CCA1-ox and *cca1lhy*. Model fitting was performed using data points from the second day onward, under the assumption that seed-derived nutrients support growth during the initial phase of the experiment. We explored a range of values for the photosynthetic rate parameter (a) from 0.01 to 0.3 and performed model fitting for each setting. All calculations were performed using Mathematica 13.1 (Wolfram Research Inc.). The source code is available at https://github.com/seki-design/sucrose-transport.

QUANTIFICATION AND STATISTICAL ANALYSIS

Statistical analyses were performed using GraphPad Prism software. For comparisons between two genotypes, an unpaired two-tailed Student's T-test was applied. To assess differences among the genotypes, a one-way ANOVA was performed followed by Dunnett's post-hoc test to compare the means of each genotype relative to the WT control, while correcting multiple comparisons. To assess the interaction between genotypes and the different growth conditions, a two-way ANOVA was conducted. Where a significant interaction was observed, simple effects analysis was performed followed by Dunnett's post-hoc test within each condition. A 0.05 was set as the threshold for significance.

CellPress
OPEN ACCESS

Supplemental figures

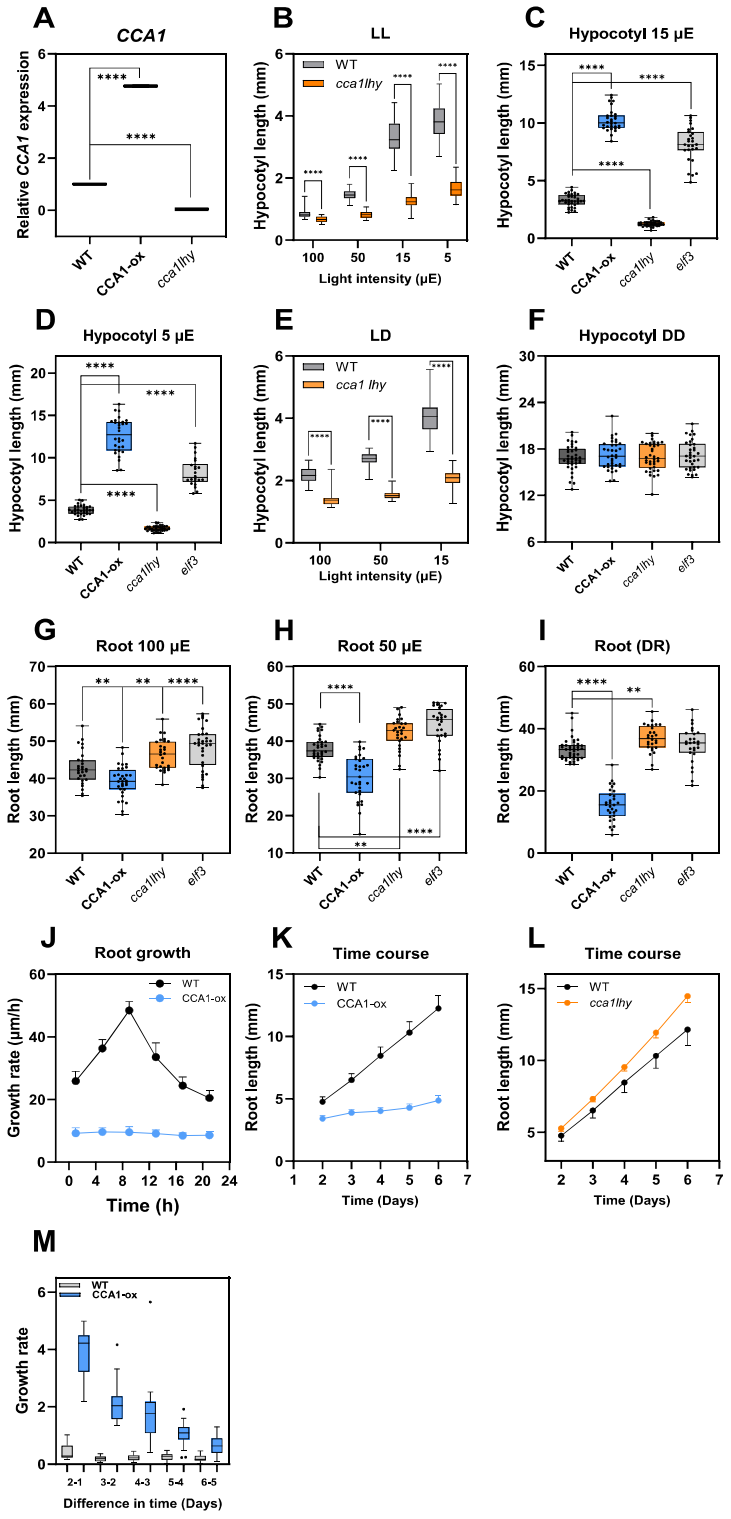

(legend on next page)

Figure S1. Organ-specific regulation of growth by CCA1, related to Figure 1

(A) Gene expression analysis by RT-qPCR of *CCA1* mRNA expression in WT, CCA1-ox, and *cca1lhy* seedlings grown under LL at 50 μE light intensity. Gene expression is graphed relative to the WT value.

(B) Hypocotyl length of WT and *cca1lhy* grown under LL at 100, 50, 15, and 5 μE light intensity.

(C and D) Hypocotyl length of WT, CCA1-ox, *cca1lhy*, and *elf3* grown under LL at (C) 15 μE or (D) 5 μE.

(E) Hypocotyl length of WT and *cca1lhy* seedlings grown under LD cycles at 100, 50, and 15 μE light intensity.

(F) Hypocotyl length of WT, CCA1-ox, *cca1lhy*, and *elf3* grown under constant darkness.

(G and H) Primary root length of WT, CCA1-ox, *cca1lhy*, and *elf3* seedlings grown at (G) 100 μE or (H) 50 μE light intensity.

(I) Primary root length of WT, CCA1-ox, *cca1lhy*, and *elf3* seedlings grown with the hypocotyls exposed to constant light (15 μE) while roots were kept in darkness (dark roots, DR).

(J) Time-course analyses of root growth over a 24-h cycle of plants grown under 15 μE of light intensity.

(K and L) Developmental time-course analyses of root growth under LL at 15 μE of (K) WT and CCA1-ox and (L) WT and *cca1lhy* (day 1 represents the day of cotyledon emergence from the seed coat).

(M) Time-course hypocotyl growth rate of WT and CCA1-ox seedlings grown under LL at 15 μE light intensity.

The boxplots display the median and interquartile range, with the whiskers extending to the data range (minimum to maximum). Three independent biological replicates were performed per experiment. **** p value $\leq$ 0.0001; ** p value $\leq$ 0.01.

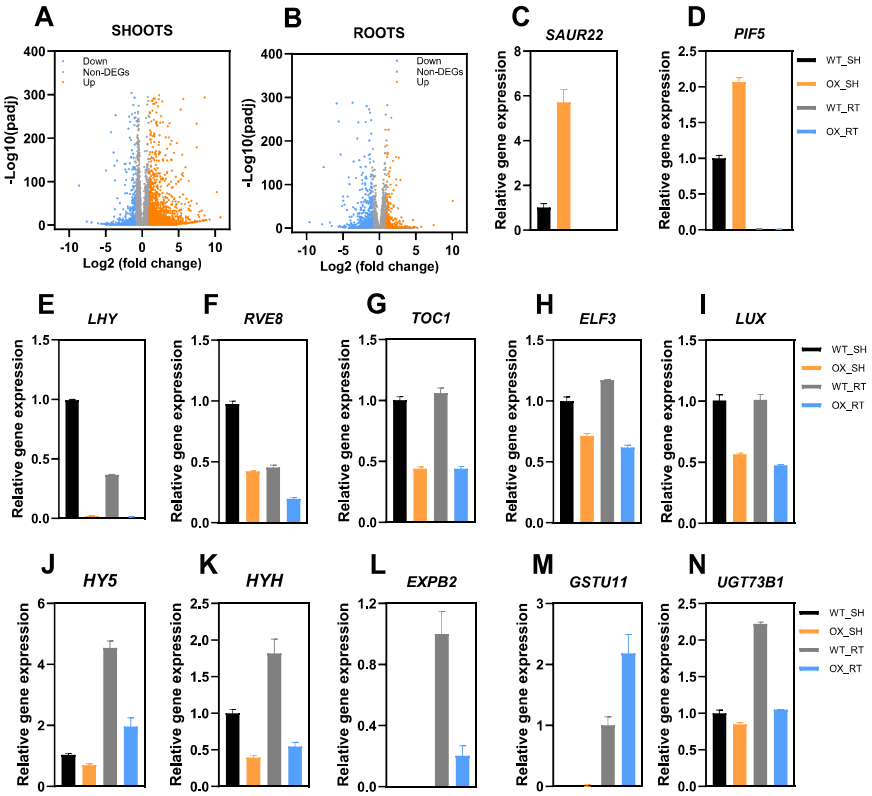

Figure S2. Organ-specific transcriptional network regulated by CCA1, related to Figure 2

(A and B) Volcano plots showing the up-, downregulated, and non-DEGs in (A) shoots and (B) roots.

(C–N) Relative RNA-seq expression analyses of (C) SAUR22, (D) PIF5, (E) LHY, (F) RVE8, (G) TOC1, (H) ELF3, (I) LUX, (J) HY5, (K) HYH, (L) EXPB2, (M) GSTU11, and (N) UGT73B1. Data are presented as the mean + SD relative to the WT value of three independent biological replicates.

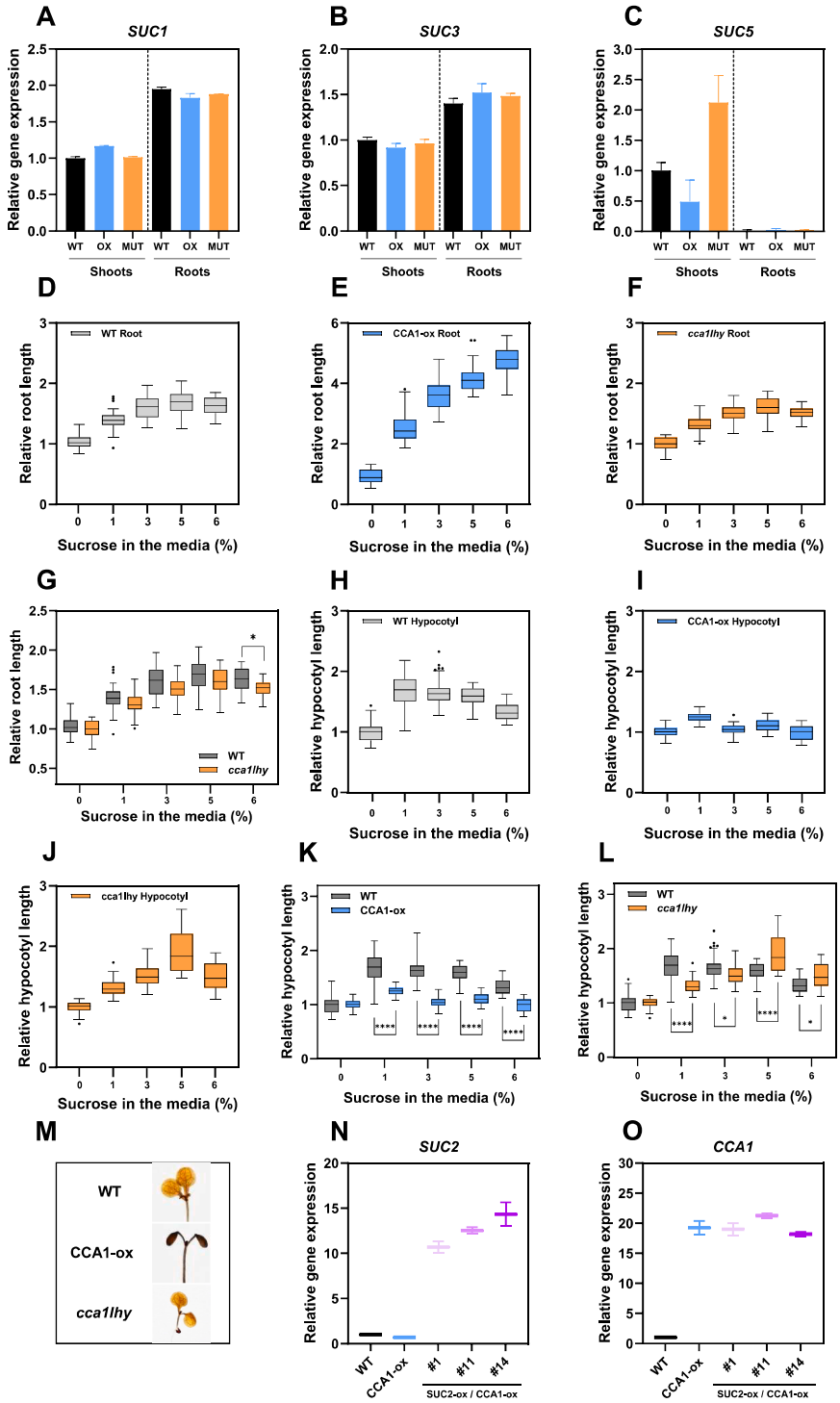

Figure S3. CCA1 represses SUC2 expression, related to Figure 3

(A–C) Relative gene expression analysis of (A) *SUC1*, (B) *SUC3*, and (C) *SUC5* expression in WT, CCA1-ox, and *cca1lhy* shoots and roots. Gene expression is graphed relative to the WT value.

(D–F) Relative root growth of (D) WT, (E) CCA1-ox, and (F) *cca1lhy* seedlings grown under LL at 15 μE with the indicated sucrose concentrations in the medium.

(G) Comparative root length of WT and *cca1lhy* seedlings grown under LL at 15 μE light intensity with varying sucrose concentrations in the medium.

(H–J) Hypocotyl growth of (H) WT, (I) CCA1-ox, and (J) *cca1lhy* seedlings grown under LL at 15 μE with the indicated sucrose concentrations in the medium.

(K and L) Comparative hypocotyl length of WT with (K) CCA1-ox and (L) *cca1lhy* seedlings grown under LL at 15 μE with the indicated sucrose concentrations in the medium. Data are presented relative to the control (0% sucrose) for each genotype.

(legend continued on next page)

(M) Starch accumulation measured by iodine staining in WT, CCA1-ox, and *cca1lhy* seedlings.
(N and O) Relative gene expression analysis by RT-qPCR of (N) *SUC2* and (O) *CCA1* expression in WT, CCA1-ox, and three SUC2-ox/CCA1-ox double over-expressing lines grown under LL at 15 μE. Gene expression is graphed relative to the WT value.
The boxplots display the median and interquartile range, with the whiskers extending to the data range (minimum to maximum). Three independent biological replicates were performed per experiment. **** p value $\leq$ 0.0001; * p value $\leq$ 0.05.

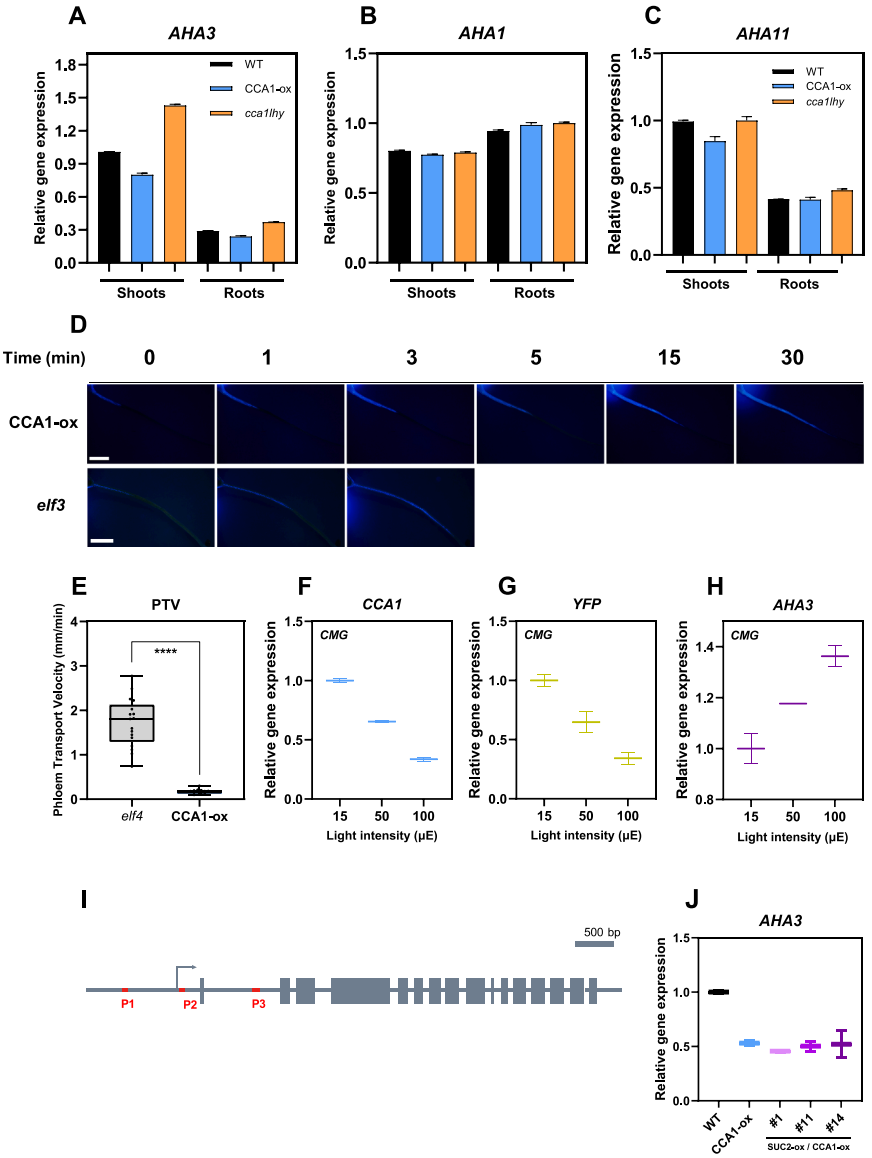

Figure S4. CCA1 controls proton electrochemical gradients in the apoplast of companion cells and impairs sucrose loading and transport velocity, related to Figure 4

(A–C) Comparative gene expression analysis by RT-qPCR of (A) *AHA3*, (B) *AHA1*, and (C) *AHA11* in shoots and roots. Gene expression is graphed as the mean ± SD relative to the WT value in shoots.

(D) Stereomicroscope images of esculin transport in CCA1-ox and *elf3* mutants at the indicated time points. Scale bar, 2 mm.

(E–H) (E) PTV in the hypocotyl of *elf4* and CCA1-ox. Relative gene expression analysis by RT-qPCR of (F) *CCA1*, (G) *YFP*, and (H) *AHA3* in CMG plants at the indicated light intensities. Gene expression is graphed relative to the value at 15 μE.

(I) Schematic diagram illustrating the genomic structure of *AHA3* and the positions of primers used for ChIP analyses.

(J) Gene expression analysis by RT-qPCR of *AHA3* in WT, CCA1-ox, and three lines of SUC2-ox/CCA1-ox. Data is graphed as the mean ± SD relative to the WT value.

The boxplots display the median and interquartile range, with the whiskers extending to the data range (minimum to maximum). Three independent biological replicates were performed per experiment.

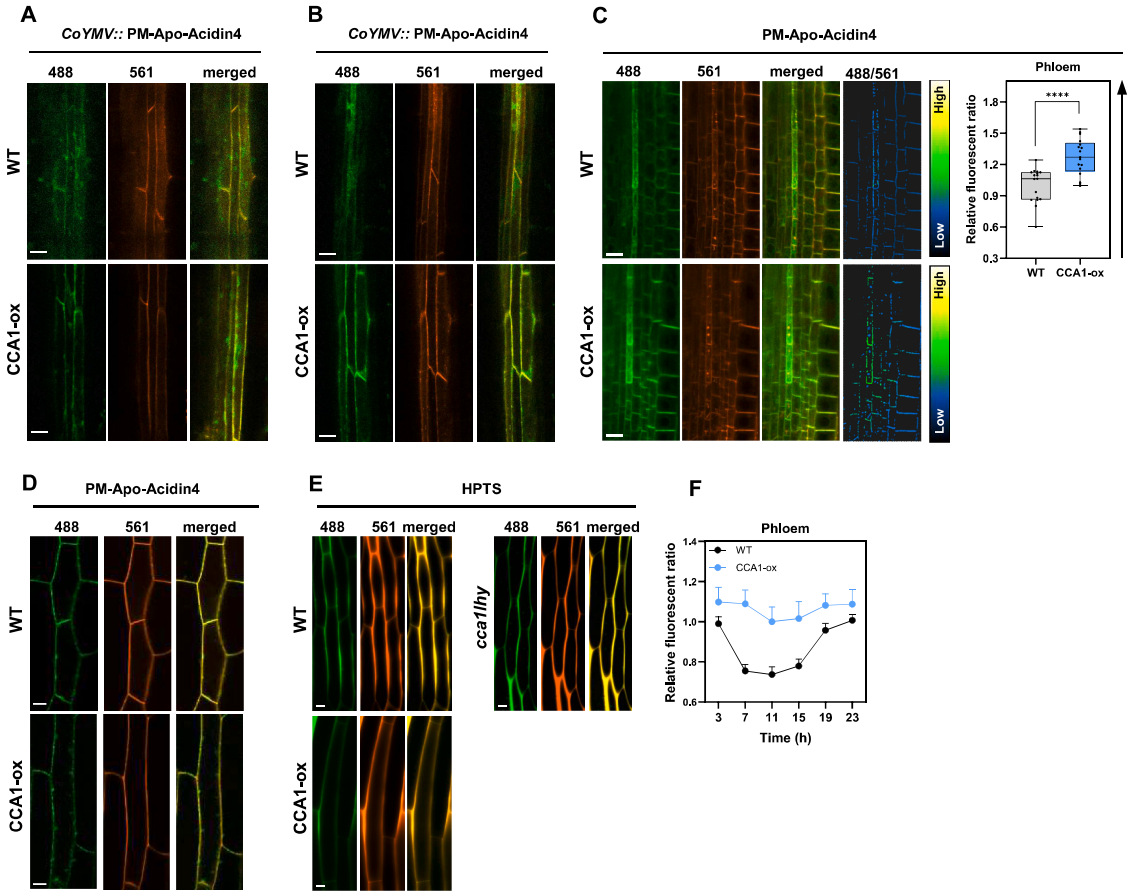

Figure S5. CCA1 controls proton electrochemical gradients in the apoplast of companion cells, related to Figure 5

(A and B) (A) Confocal images of apoplastic pH in the hypocotyl phloem using *CoYMV*::PM-Apo-Acidin4 pH sensor in WT and CCA1-ox seedlings, and (B) confocal images of apoplastic pH in the root phloem using *CoYMV*::PM-Apo-Acidin4 pH sensor in WT and CCA1-ox seedlings.

(C–E) (C) Confocal images and quantification of the apoplastic pH in companion cells of roots using PM-Apo-Acidin4 pH sensor, (D) apoplastic pH in the hypocotyl epidermal cells using PM-Apo-Acidin4 in WT and CCA1-ox seedlings, and (E) apoplastic pH in hypocotyl epidermal cells using HPTS staining.

(F) Diel (12 h light:12 h dark) time-course ratiometric analyses of apoplastic pH using PM-Apo-Acidin4 pH sensor in WT and CCA1-ox roots.

The boxplots display the median and interquartile range, with the whiskers extending to the data range (minimum to maximum). Three independent biological replicates were performed per experiment. Scale bars, 10 μm.

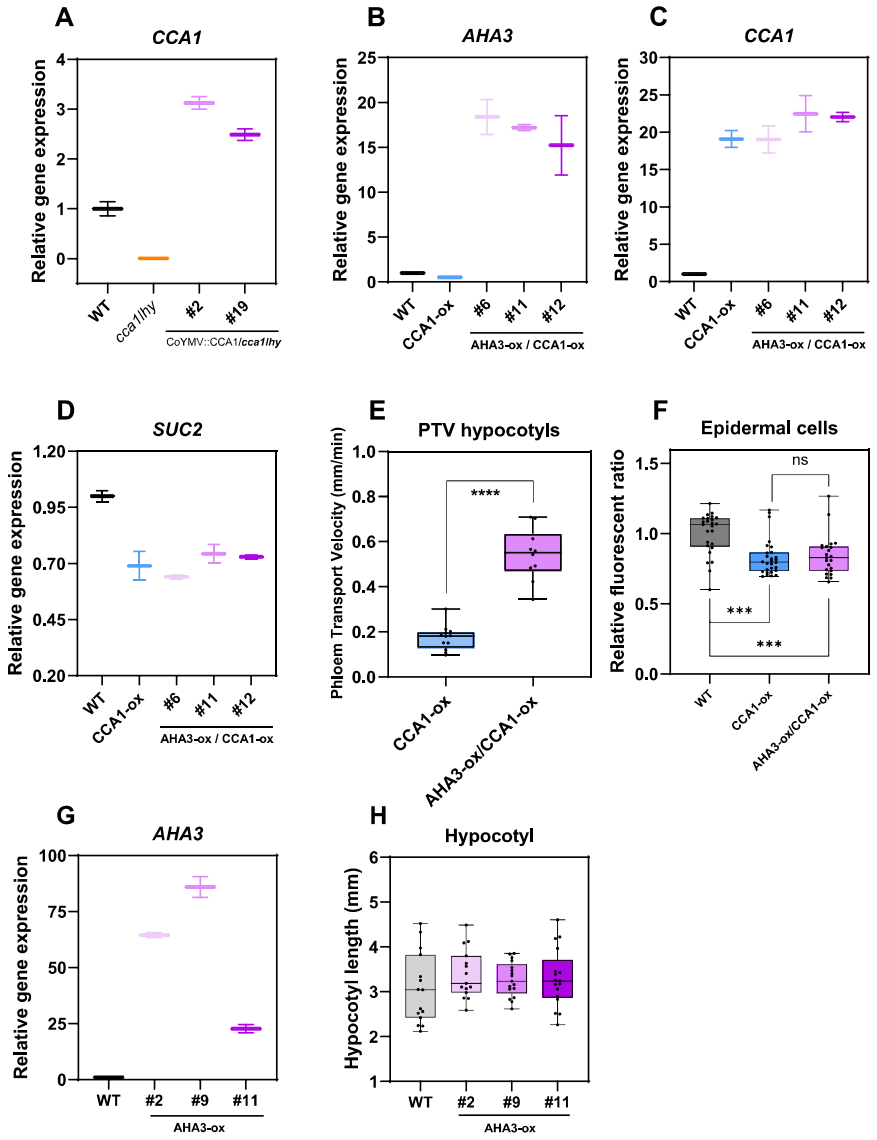

Figure S6. Restoration of growth by specific expression of CCA1 in companion cells and by overexpression of AHA3 in CCA1-ox plants, related to Figure 6

(A) Relative gene expression analysis by RT-qPCR of *CCA1* in WT, *cca1lhy*, and two *CoYMV::CCA1-YFP/cca1lhy* lines grown under LL with 15 μE light intensity.

(B–D) Relative gene expression analysis by RT-qPCR of (B) *AHA3*, (C) *CCA1*, and (D) *SUC2* in WT, CCA1-ox, and the three AHA3-ox/CCA1-ox lines. All gene expression values are graphed relative to the WT.

(E) PTV of esculin along the phloem of CCA1-ox and AHA3-ox/CCA1-ox hypocotyls.

(F) Quantification of the relative apoplastic pH in epidermal cells based on ratiometric values (488 nm/405 nm) of HPTS fluorescence.

(G) Relative gene expression analysis by RT-qPCR of *AHA3* in WT and three *AHA3*-ox lines grown under LL at 15 μE light intensity. All gene expression values are graphed relative to the WT.

(H) Hypocotyl length of WT and three *AHA3*-ox lines grown under LL at 15 μE light intensity.

The boxplots display the median and interquartile range, with the whiskers extending to the data range (minimum to maximum). Three independent biological replicates were performed per experiment.